IEEE Access
Multidisciplinary | Rapid Review | Open Access Journal

Received July 24, 2020, accepted August 1, 2020, date of publication August 5, 2020, date of current version August 18, 2020.

Digital Object Identifier 10.1109/ACCESS.2020.3014471

Wideband Hybrid Precoding Using Time Modulated Arrays

JOSÉ P. GONZÁLEZ-COMA, (Member, IEEE), AND LUIS CASTEDO, (Senior Member, IEEE)
Department of Computer Engineering and CITIC Research Center, University of A Coruña, 15001 A Coruña, Spain

Corresponding author: José P. González-Coma (jose.gcoma@udc.es)

This work was supported in part by the Xunta de Galicia under Grant ED431G2019/01; in part by the Agencia Estatal de Investigación (AEI) of Spain, under Grant TEC2016-75067-C4-1-R, Grant RED2018-102668-T, and Grant PID2019-104958RB-C42; and in part by the European Regional Development Fund (ERDF) funds of the European Union (EU) (AEI/FEDER, UE).

ABSTRACT Hybrid digital-analog precoding is a cost effective solution for transmitting over the large bandwidths and huge antenna arrays available in the millimeter wave frequency bands. In this work we focus on the transmission of wideband signals over hybrid precoders that utilize Time-Modulated Arrays in the analog domain. We consider analog precoders constructed with Single-Pole-Double-Throw switches which are both flexible and efficient. We pose two Orthogonal Frequency-Division Multiplexing symbol configurations to cope with the harmonic interference introduced by the Time-Modulated Array. One does not take advantage of the wireless channel frequency diversity and the other does. We optimize digital and analog precoders to maximize the achievable rate in both symbol configurations. Optimization takes into account the switching devices efficiency and the inherent losses of this antenna technique. Finally, we show the excellent performance obtained with the proposed approach, in terms of achievable rate, compared to that of conventional phased arrays.

INDEX TERMS Adaptive arrays, antenna arrays, energy efficiency, massive MIMO, millimeter wave communication, OFDM modulation, precoding, RF signals, wireless communication.

I. INTRODUCTION

The use of millimeter wave (mmWave) frequency bands in future wireless communication systems is promising because of the large spectrum availability. The mmWave signals experience a severe free-space pathloss that has to be compensated with the large gains obtained with massive Multiple-Input Multiple-Output (MIMO) antenna arrays [1]. To alleviate the huge costs and power consumption associated to massive MIMO arrays, hybrid digital-analog architectures are helpful because they reduce the number of Radio Frequency (RF) chains [2].

Prior art considers different analog networks connecting the RF chains and the array elements [3]. Consequently, the feasible set of analog precoding matrices depends on the particular features of the analog network. The canonical approach consists in the use of phased arrays implemented with Phase Shifters (PSs). These phased arrays present a frequency flat response, unveiling the necessity of new hybrid precoding solutions for the wideband scenario, e.g. [4]–[12].

The associate editor coordinating the review of this manuscript and approving it for publication was Gerard-Andre Capolino.

In particular, authors in [4]–[6], [9] exploit the common channel subspace for different frequencies. While [4] performs a search over the candidate set of precoders, [5]–[7], [9] perform a channel decomposition to identify the most promising angular directions. Other solutions include machine learning techniques to obtain the hybrid precoders, like [10], [11].

Some works further reduce the power consumption by considering limited resolution PSs [7], [10], [12] or partially connected structures [12], at the expense of smaller array gains. Nevertheless, none of the previous works contemplate the large Insertion Lossess (ILs) introduced by the PSs. Further, such ILs linearly increase with the carrier frequency which leads to large losses in mmWave [13]. To compensate for these losses Power Amplifiers (PAs) are often employed. Nonetheless, PAs lead to their own ILs, power consumption, and larger chip areas [14].

Time-Modulated Arrays (TMAs) use RF switches governed by periodical pulses, and constitute an appealing alternative for mmWave analog implementations in terms of cost, ILs, and chip areas (see [15] for a detailed analysis). As counterpart, TMAs radiate the transmitted signal over

the harmonics of the carrier frequency, a drawback known as Sideband Radiation (SR). Besides the power wasted, SR imposes stringent limitations on the signal bandwidth [16].

Conventional TMAs, implemented with Single-Pole-Single-Throw (SPST) switches, are rather inefficient due to the power absorption during the off-state. To overcome this limitation, Single-Pole-Double-Throw (SPDT) switches have been considered in the literature (see e.g. [17]–[23]). The rigid antenna weighting patterns in [17] prevent for adaptation to channel conditions. Conversely, a relatively flexible scanning is possible using TMAs provided in [18]–[22] operating in phased array mode, but approaches in [18], [19] require two antenna arrays working simultaneously. Recently, authors in [21], [22] investigated the use of stair-step pulses to further increase the available bandwidth for the data signal by a factor of 8. Nevertheless, the analog devices and connections in [20]–[22] complicate the circuitry, increase the ILs due to signal splitting, and result in larger chip areas. Moreover, approaches in [17]–[23] do not support arbitrarily large data signal bandwidths.

Another promising research direction to avoid PS ILs arose in the context of cloud radio access networks for radio over fiber systems [24]. Therein, authors design analog precoders relying on fiber non-linearity, enabling similar scanning capabilities as a phased array. The main disadvantages are the limitations on the angular range and the phase inaccuracy introduced by the optical devices.

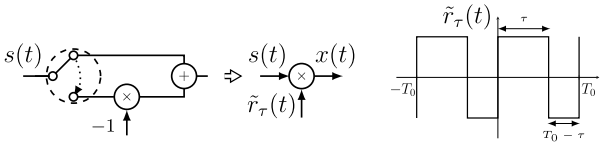

FIGURE 1. Proposed TMA element using a SPDT switch.

In this work, contrary to prior art [18]–[22], we consider the fundamental mode to transmit the data signal. Hence, the antenna excitation resulting from the posed scheme of Fig. 1 is real valued. As such, we adapt the pulse durations to perform analog precoding. This procedure is radically different from that in prior work, which uses fixed pulse durations and progressive pulse delays in the antenna elements to implement the analog precoder. Furthermore, contrary to the aforementioned work we incorporate the baseband precoder to improve the flexibility, i.e., we perform hybrid precoding.

Due to the harmonic replicas, wideband signals transmitted with TMAs suffer a destructive frequency overlapping, denoted as Harmonic Interference (HI). To cope with the HI, we provide an adaptation of the Orthogonal Frequency-Division Multiplexing (OFDM) modulation to preserve the data subcarriers from the HI. We propose two OFDM symbol configurations. In the former, OFDM parameters are chosen to completely remove the HI from the useful subcarriers. In the latter configuration, the HI will be employed to exploit the channel frequency diversity.

The singular characteristics of the proposed analog network and modulation prevents the application of previous hybrid precoding solutions. Therefore, we design hybrid precoders to maximize the average per-subcarrier achievable rate. Different designs will be considered for the two previous OFDM symbol configurations. In the first one, hybrid precoders concentrate the radiated power on the fundamental mode while minimizing the SR. In the second configuration, some useful harmonics are jointly considered in the design. Further, we include the hardware efficiency in the transmit power constraint of both OFDM symbol configurations.

Finally, we make a comparison, in terms of power consumption and ILs, between the proposed TMA-based analog network and the conventional one built using PSs. This analysis enables a fair comparison in our numerical simulations.

The contributions of this work are summarized as follows:

- We propose a simple TMA-based analog network built with SPDT switches that presents high power efficiency.
- Symbols are modulated at baseband to combat the HI introduced by the TMA.
- Based on the proposed TMA and OFDM symbol configurations, we design the hybrid precoders.
- We analyze the ILs and power consumption of proposed SPDT TMA and PS analog networks.

II. TIME-VARIANT SPDT TMA ANALOG PRECODING

Let us consider a point-to-point wireless link where a transmitter with M antennas sends a wideband OFDM modulated signal to a single-antenna receiver. Prior to its transmission, the OFDM signal is precoded with a hybrid digital-analog precoder having $N_{\text{RF}} \ll M$ RF chains and a fully connected analog network, i.e., all the antennas are connected to all the RF chains.

In the analog domain, we will use a TMA implemented with SPDT switches as shown in Fig. 2. The working principle of the proposed SPDT time modulator is the following. During a switching cycle $0 < t < T_0$, the SPDT switch is connected to the upper throw during a time duration $0 < \tau < T_0$ and to the lower throw during the complementary time $T_0 - \tau > 0$. The signal driven to the lower throw is sign reversed. Finally, the signal fed to the antenna is the sum of the two throws. The overall switching operation is repeated periodically each T_0. The effect of this switching operation is to time modulate the RF signal passing through with the bipolar square periodic signal plotted in Fig. 1.

In order to mathematically analyze the proposed SPDT time modulation, let $\tilde{r}_\tau(t)$ be the periodic (T_0) bipolar pulse. The coefficients of the exponential Fourier series representation of $\tilde{r}_\tau(t)$ are

$$R^q = \frac{1}{T_0}\int_0^{T_0} \tilde{r}_\tau(t) \mathrm{e}^{-jq\omega_0 t} dt = \begin{cases} 2\xi - 1 & q = 0 \\ 2\xi\, \mathrm{sinc}(\pi q \xi)\mathrm{e}^{-j\pi q\xi} & q \neq 0 \end{cases} \quad (1)$$

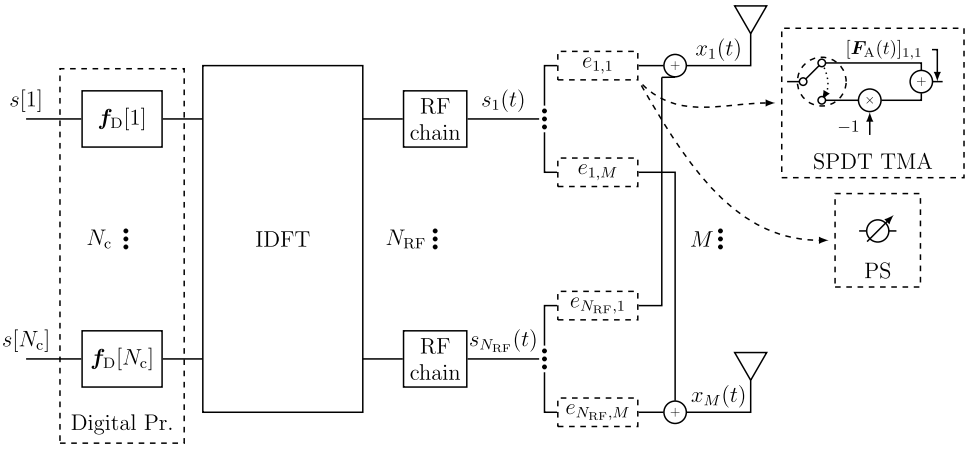

FIGURE 2. Wideband hybrid precoding block diagram showing two possible analog networks: proposed SPDT TMA and conventional phased array.

with $\omega_0 = \frac{2\pi}{T_0}$ the fundamental switching frequency (rad/s), $\xi = \frac{\tau}{T_0}$ the normalized pulse duration, and $\mathrm{sinc}(x) = \frac{\sin(x)}{x}$. The proposed scheme enables also time-delayed versions, $\tilde{r}_\tau(t-\varrho)$, by simply changing the initial switching instant to $\varrho \in [0, T_0]$.

Let $\tilde{r}_{\tau_{m,r}}(t-\varrho_{m,r})$ be the signal that time modulates the wideband RF signal $s_r(t)$, with central frequency ω_c, passing through the branch connecting the r-th RF chain output with the m-th antenna. Thus, the time-modulated signal that enters the m-th antenna is

$$x_m(t) = \sum_{r=1}^{N_{\mathrm{RF}}} \tilde{r}_{\tau_{m,r}}(t-\varrho_{m,r}) s_r(t). \tag{2}$$

Using matrix-vector notation, the previous input-output relationship can be rewritten as

$$\boldsymbol{x}(t) = \boldsymbol{F}_{\mathrm{A}}(t)\boldsymbol{s}(t), \tag{3}$$

where $\boldsymbol{s}(t) \in \mathbb{C}^{N_{\mathrm{RF}}}$ and $\boldsymbol{x}(t) \in \mathbb{C}^{M}$ are vectors comprising the signals $s_r(t)$ and $x_m(t)$, respectively, and $\boldsymbol{F}_{\mathrm{A}}(t) \in \mathbb{C}^{M\times N_{\mathrm{RF}}}$ is the time-variant analog precoding matrix whose entries are $[\boldsymbol{F}_{\mathrm{A}}(t)]_{m,r} = \tilde{r}_{\tau_{m,r}}(t-\varrho_{m,r})$. Further, $\boldsymbol{F}_{\mathrm{A}}(t)$ can be represented by its exponential Fourier series expansion

$$\boldsymbol{F}_{\mathrm{A}}(t) = \sum_{q=-\infty}^{\infty} \boldsymbol{F}_{\mathrm{A}}^{q} \mathrm{e}^{jq\omega_0 t}, \tag{4}$$

where

$$\boldsymbol{F}_{\mathrm{A}}^{q} = \begin{bmatrix} [\boldsymbol{F}_{\mathrm{A}}^{q}]_{1,1} & \cdots & [\boldsymbol{F}_{\mathrm{A}}^{q}]_{1,N_{\mathrm{RF}}} \\ \vdots & \ddots & \vdots \\ [\boldsymbol{F}_{\mathrm{A}}^{q}]_{M,1} & \cdots & [\boldsymbol{F}_{\mathrm{A}}^{q}]_{M,N_{\mathrm{RF}}} \end{bmatrix} \tag{5}$$

is a $M \times N_{\mathrm{RF}}$ matrix containing the q-th harmonic Fourier series coefficients of all the analog precoder time modulating signals. Using the result in (1), the entries in $\boldsymbol{F}_{\mathrm{A}}^{q}$ are readily obtained as

$$[\boldsymbol{F}_{\mathrm{A}}^{q}]_{m,r} = R_{m,r}^{q} \mathrm{e}^{-jq\omega_0\varrho_{m,r}}. \tag{6}$$

For the fundamental mode (i.e., $q = 0$), we obtain $[\boldsymbol{F}_{\mathrm{A}}^{0}]_{m,r} = (2\xi_{m,r} - 1) \in [-1, 1]$. Therefore, we denote by $\mathcal{F}$ the set of matrices with real-valued entries within the interval $[-1, 1]$. Accordingly, the feasible set of analog precoders, $\boldsymbol{F}_{\mathrm{A}}^{0} \in \mathcal{F}$, is convex. This feature is in contrast to TMA approaches performing a phase weighting of the antenna elements in, e.g. [19], [20], and allows us to formulate analog precoding design problems as convex problems.

Using (4), transmitted signal in (3) can be rewritten as

$$\boldsymbol{x}(t) = \sum_{q=-\infty}^{\infty} \boldsymbol{F}_{\mathrm{A}}^{q} \boldsymbol{s}(t) \mathrm{e}^{jq\omega_0 t}. \tag{7}$$

This equation reveals that the TMA radiates the RF signal $\boldsymbol{s}(t)$ centered at ω_c, but also replicas at the harmonic frequencies $\omega_c + q\omega_0$, $q \in \mathbb{Z}$. The signal radiated over the harmonics $q \neq 0$, termed SR, is usually unexploited.

The existence of SR is a distinctive feature of TMAs, and will be considered an undesirable effect for three main reasons. The first is that it interferes into the adjacent channels. The second is that the power due to SR is wasted and thus reduces the TMA power efficiency. And the third is that the SR replicas may overlap in frequency with the useful signal causing HI.

Assuming the baseband bandwidth of $\boldsymbol{s}(t)$ is $B_{\boldsymbol{s}}$ Hz, SR replicas do not overlap in frequency as long as the switching fundamental frequency $f_0 = \frac{1}{T_0}$ Hz satisfies the constraint $2f_0 > B_s$ [16]. This is a serious hindrance when transmitting wideband signals because the maximum f_0 is severely limited by the SPDT switching technology. Typical values of T_0 for SPDTs switches are about a few μs, with switching speeds in the order of ns [17], [25]. These values are fully compatible with channel coherence times of about 1 ms, reported for a carrier frequency of 60 GHz at a 800 Hz Doppler shift [26].

III. WIDEBAND TRANSMISSION MODEL

Let us consider the wideband transmission of data symbols using an OFDM modulation with N_c subcarriers.

The bandwidth of the OFDM modulated signal is $B_{\text{OFDM}} = \frac{1}{T_s}$ where T_s is the sampling period. Correspondingly, the duration of an OFDM symbol is $T_{\text{OFDM}} = N_c T_s$ and the subcarrier spacing $\frac{1}{N_c T_s}$.

Let $s[\ell]$ be the data symbol transmitted over the ℓ-th subcarrier. According to Fig. 2, the data symbols are linearly processed using the frequency selective baseband precoders $\boldsymbol{f}_{\text{D}}[\ell] \in \mathbb{C}^{N_{\text{RF}}}$. In order to adequately transmit the precoded signal over the analog network, we propose to expand the OFDM subcarriers in the frequency domain by the integer factor $\Delta_f \in \mathbb{Z}^+$. Hence, the discrete-time representation of the digitally precoded OFDM vector symbol $\boldsymbol{s}\langle n\rangle \in \mathbb{C}^{N_{\text{RF}}}$ is

$$\boldsymbol{s}\langle n\rangle = \sum_{\ell=0}^{L-1} \boldsymbol{f}_{\text{D}}[\ell] s[\ell] \mathrm{e}^{\mathrm{j}\frac{2\pi \ell \Delta_f n}{N_c}}, \quad n = 0, 1, \ldots, N_c - 1, \quad (8)$$

where $L = \lfloor \frac{N_{\text{c}}}{\Delta_f} \rfloor$ is the effective number of transmitted data symbols within an OFDM symbol. Observe that (8) can be interpreted as an OFDM symbol of size N_c with the data symbols $s[\ell]$ separated by $\Delta_f - 1$ zeros. The motivation for expanding the subcarrier separation is to accommodate the harmonic replicas created by the TMA analog precoder such that they do not interfere the data symbols. The expansion by Δ_f also causes $\boldsymbol{s}\langle n\rangle$ to become periodic. Indeed, $\boldsymbol{s}\langle n\rangle$ contains Δ_f repetitions such that $\boldsymbol{s}\langle n\rangle = \boldsymbol{s}\langle n + L\rangle$ for $0 \leq n < L$.

Note that, when $\Delta_f > 1$, the subcarriers set to zero are not employed for data transmission. This releases resources in the OFDM signal that can be used for other purposes like reducing the symbol period T_{OFDM}, exploiting the redundancy in $\boldsymbol{s}\langle n\rangle$, inserting pilots for channel estimation, or accommodating other users in an Orthogonal Frequency-Division Multiple Access (OFDMA) system [27]. All these approaches require a detailed analysis that is out of the scope of this work. Nevertheless, in Sec. V-B we employ these resources to exploit the frequency diversity of the channel.

We now consider that the digitally precoded discrete-time OFDM symbol $\boldsymbol{s}\langle n\rangle$ in (8) modulates the amplitude of a continuous-time pulsed waveform $p(t) = \frac{1}{\sqrt{T_s}} \operatorname{sinc}(t/T_s)$ to produce the continuous-time vector signal

$$\boldsymbol{s}(t) = \sum_{n=0}^{N_{\text{c}}-1} \boldsymbol{s}\langle n\rangle p(t - nT_s). \quad (9)$$

Note that the autocorrelation $g(t) = p(t) * p(-t)$ fulfills the Nyquist zero Inter-Symbol Interference (ISI) criterion. As usual in OFDM [28], we now introduce the following u-th base function for the frequency index $v = \Delta_f \ell$

$$\varphi_v(t) = \sum_{n=0}^{N_{\text{c}}-1} \mathrm{e}^{\mathrm{j}\frac{2\pi vn}{N_{\text{c}}}} p\left(t - nT_s\right), \quad (10)$$

which constitutes an orthogonal set on the subindex v.

In the analog domain, $\boldsymbol{s}(t)$ is precoded by $\boldsymbol{F}_{\text{A}}(t)$ to produce $\boldsymbol{x}(t)$, as in (7). Moreover, we set the OFDM sampling period T_s as a fraction of the fundamental period T_0, i.e., $T_0 = NT_s$ with $N \in \mathbb{Z}^+$. We now introduce the integer factor $\Delta_t \in \mathbb{Z}^+$ and configure $N_c = \Delta_t N$. Therefore, the OFDM symbol duration, $T_{\text{OFDM}} = \Delta_t T_0$, and the frequency separation between the N_c subcarriers, $\frac{1}{\Delta_t T_0}$, can be adjusted according to the channel conditions.

To further describe $\boldsymbol{x}(t)$ we first note that, at the receiver side, we will employ the matched filter $p(-t)$ whose bandwidth is $\frac{1}{T_s}$. This means that only the harmonic frequencies meeting the inequality $-\frac{1}{2T_s} \leq qf_0 \leq \frac{1}{2T_s}$ (i.e., $|q| \leq \frac{N}{2}$) pass through $p(-t)$, irrespective of the channel response. Therefore, from the receiver perspective, the Fourier series expansion of $\boldsymbol{F}_{\text{A}}(t)$ can be truncated as

$$\boldsymbol{F}_{\text{A}}(t) = \sum_{|q| \leq \frac{N}{2}} \boldsymbol{F}_{\text{A}}^q \mathrm{e}^{jq\omega_0 t}. \quad (11)$$

Thus, combining (7), (9) and (11), the useful radiated signal $\boldsymbol{x}_u(t)$, i.e., the signal radiated over the receiver bandwidth, can be represented as

$$\begin{aligned}
\boldsymbol{x}_u(t) &= \sum_{n=0}^{N_{\text{c}}-1} \sum_{|q| \leq \frac{N}{2}} \boldsymbol{F}_{\text{A}}^q \boldsymbol{s}\langle n\rangle \mathrm{e}^{jq\omega_0 nT_s} p(t - nT_s) \\
&= \sum_{n=0}^{N_{\text{c}}-1} \sum_{|q| \leq \frac{N}{2}} \sum_{\ell=0}^{L-1} \boldsymbol{F}_{\text{A}}^q \boldsymbol{f}_{\text{D}}[\ell] s[\ell] \mathrm{e}^{\frac{\mathrm{j}2\pi a(q,\ell)n}{N_{\text{c}}}} p(t - nT_s) \\
&= \sum_{n=0}^{N_{\text{c}}-1} \sum_{i=0}^{N_{\text{c}}-1} \boldsymbol{x}_u[i] \mathrm{e}^{\frac{\mathrm{j}2\pi in}{N_{\text{c}}}} p(t - nT_s), \quad (12)
\end{aligned}$$

where $a(q, \ell) = \Delta_t q + \Delta_f \ell$ is an auxiliary function that determines the subcarrier index for the ℓ-th data symbol and the q-th harmonic replica, such that $0 \leq a(q, \ell) < N_{\text{c}}$, and

$$\boldsymbol{x}_u[i] = \sum_{(q,\ell) \in \mathcal{H}_i} \boldsymbol{F}_{\text{A}}^q \boldsymbol{f}_{\text{D}}[\ell] s[\ell] \in \mathbb{C}^M \quad (13)$$

is the effective vector symbol transmitted over the i-th subcarrier. $\mathcal{H}_i$, $i \in \{0, \ldots, N_{\text{c}} - 1\}$, is the set of tuples (q, ℓ) containing the data ℓ and harmonic q indices associated to the i-th subcarrier, and is given by

$$\mathcal{H}_i = \left\{ (q, \ell) \,|\, a(q, \ell) = i, 0 \leq \ell \leq L - 1, \ |q| \leq \frac{N}{2} \right\}. \quad (14)$$

A. CHANNEL MODEL

The transmitted vector signal $\boldsymbol{x}(t)$ inputs the wireless channel to produce the received signal. We consider the Saleh-Valenzuela propagation model [29] with N_{p} propagation paths. Assuming a single receive antenna, the continuous-time channel impulse response is

$$\boldsymbol{h}(t) = \sum_{l=1}^{N_{\text{p}}} \alpha_l \delta(t - z_l) \boldsymbol{a}(\vartheta_l, f), \quad (15)$$

where α_l and z_l are the complex gain and time delay, respectively, and $\boldsymbol{a}(\vartheta_l, f)$ is the frequency dependent steering vector pointing toward the Angle of Departure (AoD) ϑ_l, for the l-th propagation path. Assuming a Uniform Linear Array (ULA)

with inter-antenna distance equal to half of the wavelength, the steering vectors have the form

$$\boldsymbol{a}(\vartheta_l, f) = [1, \mathrm{e}^{-\mathrm{j}\pi \frac{f}{f_c}\sin\vartheta_l}, \ldots, \mathrm{e}^{-\mathrm{j}\pi \frac{f}{f_c}\sin\vartheta_l (M-1)}]^T, \quad (16)$$

where $f_c = \frac{\omega_c}{2\pi}$ is the carrier frequency in Hz. Note that this steering vector model accounts for the so-called beam squint effect [30].

For the sake of notation simplicity, we introduce the discrete-time equivalent channel response that includes the combined effects of the transmit and receive shaping filters. That is, sampling $\boldsymbol{h}(t) * g(t)$ at the sampling rate $1/T_s$ produces the equivalent discrete-time channel impulse response

$$\boldsymbol{h}\langle n\rangle = \sum_{l=1}^{N_\mathrm{p}} \alpha_l g(nT_s - z_l)\boldsymbol{a}(\vartheta_l, f), \quad n = \{0, \ldots, D-1\} \quad (17)$$

where z_{N_p} is the channel delay spread.

B. WIDEBAND RECEIVED SIGNAL

In OFDM, a cyclic prefix is introduced to suppress ISI and Inter-Carrier Interference (ICI). OFDM symbols are cyclically extended with $D-1$ samples as $\bar{\boldsymbol{s}}\langle n\rangle = \boldsymbol{s}\langle n+N_\mathrm{c}\rangle$ for $n = -D+1, \ldots, -1$ and $\bar{\boldsymbol{s}}\langle n\rangle = \boldsymbol{s}\langle n\rangle$ for $n = 0, \ldots, N_\mathrm{c}-1$. For the transmitted signal vector $\boldsymbol{x}(t)$, these samples are affected by the analog precoder to produce

$$\begin{aligned}\bar{\boldsymbol{x}}(t) &= \sum_{n=-D+1}^{N_\mathrm{c}-1} \sum_{|q|\le \frac{N}{2}} \boldsymbol{F}_\mathrm{A}^q \bar{\boldsymbol{s}}\langle n\rangle \mathrm{e}^{jq\omega_0(n+D-1)T_s} p(t-nT_s) \\ &= \sum_{n=-D+1}^{N_\mathrm{c}-1} \sum_{|q|\le \frac{N}{2}} \bar{\boldsymbol{F}}_\mathrm{A}^q \bar{\boldsymbol{s}}\langle n\rangle \mathrm{e}^{jq\omega_0 nT_s} p(t-nT_s), \end{aligned} \quad (18)$$

where $\bar{\boldsymbol{F}}_\mathrm{A}^q = \boldsymbol{F}_\mathrm{A}^q \mathrm{e}^{jq\omega_0(D-1)T_s}$. Observe that, thanks to the periodicity of $\boldsymbol{F}_\mathrm{A}(t)$, the structure of the cyclic prefix is not compromised. This is a consequence of our design decisions $T_s = T_0/N$ and N_c being an integer multiple of N. Also, a side effect of including the cyclic prefix is the unit-modulus scaling factor affecting $\boldsymbol{F}_\mathrm{A}^q$. Nevertheless, this scalar factor is transparent to the power constraint and the performance metric.

Consider now the effective symbols $\boldsymbol{x}_u[i]$ described in (13). As in conventional OFDM, we apply the basis function $\varphi_v^*(-t)$ of (10) to obtain the received symbol vector

$$\begin{aligned} y[v] &= \sum_{n=0}^{D-1} \boldsymbol{h}^\mathrm{H}\langle n\rangle \boldsymbol{x}_u[v] \mathrm{e}^{-\frac{\mathrm{j}2\pi vn}{N_\mathrm{c}}} + n[v] \\ &= \boldsymbol{h}^\mathrm{H}[v]\boldsymbol{x}_u[v] + n[v], \end{aligned} \quad (19)$$

where $\boldsymbol{h}^\mathrm{H}[v] = \sum_{n=0}^{D-1} \boldsymbol{h}^\mathrm{H}\langle n\rangle \mathrm{e}^{\frac{-\mathrm{j}2\pi vn}{N_\mathrm{c}}}$ is the channel frequency response at the v-th subcarrier and $n[v] \sim \mathcal{N}_\mathbb{C}(0, \sigma^2)$ is the noise. Note how thanks to the cyclic prefix there is no ISI and ICI in (19) and $\boldsymbol{x}_u[v]$ is simply recovered by removing the effect of $\boldsymbol{h}^\mathrm{H}[v]$.

It is then clear that the motivation for introducing the integer factors Δ_t and Δ_f in the OFDM configuration is twofold: adapting the OFDM symbol to the channel conditions while preserving the structure of the cyclic prefix; and adjusting the amount of HI. In the ensuing sections we consider different choices of Δ_f and Δ_t to achieve different per-symbol SNRs and HI levels.

IV. PRECODING DESIGN FUNDAMENTALS

In this section we address two precoding design fundamental issues. One is the way the proposed TMA precoder manage the total power available in transmission, in comparison with a phased array, and the other is the particular problem formulation for the proposed analog network.

A. TOTAL POWER AVAILABLE IN TRANSMISSION

Recall that, due to the use of our proposed SPDT TMA analog precoder, the overall radiated signal $\boldsymbol{x}(t)$ given by (7) contains the sideband harmonic replicas. Thus, the total transmitted power is

$$P_\mathrm{TX}^\mathrm{TMA} = \sum_{\ell=0}^{L-1} \sum_{q=-\infty}^{\infty} \|\boldsymbol{F}_\mathrm{A}^q \boldsymbol{f}_\mathrm{D}[\ell]\|_\mathrm{F}^2. \quad (20)$$

where $\|\cdot\|_\mathrm{F}^2$ represents the Frobenius norm. Considering that the useful power is the one radiated over the fundamental mode $q = 0$, while the remaining is wasted [15], [16], the TMA power efficiency is

$$\eta^\mathrm{TMA} = \frac{\sum_{\ell=0}^{L-1} \|\boldsymbol{F}_\mathrm{A}^0 \boldsymbol{f}_\mathrm{D}[\ell]\|_\mathrm{F}^2}{P_\mathrm{TX}^\mathrm{TMA}}. \quad (21)$$

Clearly, achieving a high value of η^TMA is essential for the feasibility of TMA analog precoding in a practical setting.

Analyzing the total power consumption of a hybrid precoder is rather difficult due to the large number of RF elements and connections in the analog precoding network. Instead, we determine the power savings achieved with the proposed TMA analog network when compared to a conventional phased array implemented with high-resolution PSs.

Let P_TOT be the total power available in transmission no matter the analog scheme. P_TOT is decomposed as

$$P_\mathrm{TOT} = P_\mathrm{TX} + P_\mathrm{HW}, \quad (22)$$

where P_TX is the radiated power and P_HW the power consumed by the hardware. In the following, we will use the superindices $^\mathrm{PS}$ and $^\mathrm{TMA}$ to refer to the analog networks implemented with conventional PSs and the proposed TMA. Assuming the total power available is the same in both approaches, the TMA radiated power is

$$P_\mathrm{TX}^\mathrm{TMA} = P_\mathrm{TX}^\mathrm{PS} + P_\mathrm{HW}^\mathrm{PS} - P_\mathrm{HW}^\mathrm{TMA}. \quad (23)$$

This way we can perform fair comparisons between different methods by accounting for their specific efficiencies and hardware consumptions, since the total power available in transmission is the same.

Circuitry simplicity is one of the strengths of the proposed TMA analog network, compared to that of wideband

TMAs [18]–[22]. However, PS-based phased arrays are even simpler, since they just include the PS and the PA to compensate the large IL introduced by the PS.

The ILs of a PS highly depend on the underlying technology, the angular resolution, and the operating frequency, among others (see [31] for a comprehensive review). PS implementations with active devices will be discarded because they exhibit greater power consumption (around 100 mW [32]) and limited linearity performance [32]. Typical IL values for 4-bit resolution passive PSs range between -4 and -8 dB for the Ka-band (33 GHz) and the W-band (60 GHz) [3], [15], [33], but even larger losses have been reported [32]. These losses must be compensated with PAs. Leaving aside the power inefficiency and consumption of these PAs, we will use a rather optimistic IL value of -5 dB for the characterization of 4-bit PSs and a reference value of 30 mW for its hardware power consumption [3], [34].

For the proposed TMA analog precoder, there exists commercial SPDT switches with almost negligible hardware power consumption <0.5 mW and extremely low IL of about 0.3 dB. Furthermore, theses losses are independent of the working frequency and valid for large bandwidths of several GHz [25]. In addition, consider waveguide-based spatial passive combiners to add the SPDT outputs, with only a 0.2 dB IL [35], [36]. In total, the IL per TMA element are approximated by $-0.3-0.2=-0.5$ dB.

Hence, the TMA radiated power (23) in Watts is given by

$$P_{\mathrm{TX}}^{\mathrm{TMA}} = 10^{-0.05}\left(10^{0.5}P_{\mathrm{TX}}^{\mathrm{PS}} + MN_{\mathrm{RF}}(30-0.5)10^{-3}\right) \quad (24)$$

where the second addend comes from the difference $P_{\mathrm{HW}}^{\mathrm{PS}} - P_{\mathrm{HW}}^{\mathrm{TMA}}$ which is always positive because the hardware power consumption of PSs is significantly larger than that of the switching devices. Therefore, for given total power available, TMA analog networks are able to radiate significantly more power. In addition, note from (24) that the superior radiation performance of TMA versus PS networks scales linearly with the number of antennas and the operation frequency. These features make our TMA approach appealing for scenarios deploying massive antenna arrays working at mmWave.

TABLE 1. TMA power savings (mW) for different configurations.

	$M=64$	$M=128$	$M=256$	$M=512$	$M=1024$
$N_{\mathrm{RF}}=4$	7.64	15.36	30.72	61.44	122.88
$N_{\mathrm{RF}}=8$	15.36	30.72	61.44	122.88	245.76

For instance, we show in Table 1 the power savings of the proposed analog network compared to a phased array for different number of antennas, M, and RF chains, N_{RF}. For reference transmit power P_{TX} of 1 W [12], using our scheme for $M=1024$ and $N_{\mathrm{RF}}=8$ provides about 25% extra transmit power with identical total power consumption P_{TOT}.

B. PROBLEM FORMULATION

Note from (13) and (14) that the effective symbol $\boldsymbol{x}_u[i]$ with $\mathrm{mod}\,(i,\Delta_f)=0$ contains the data symbol $s[i/\Delta_f]$ and the HI caused by the time variant analog precoders. This interference is characterized by the tuples of harmonic and data symbol indices $(q,\ell)\in\mathcal{H}_i$ of (14), with $q\neq 0$. Furthermore, when $\Delta_f>1$ the harmonic replicas "fill" the j subcarriers satisfying $\mathrm{mod}\,(j,\Delta_f)\neq 0$ with HI corresponding to the indices $(q,\ell)\in\mathcal{H}_j$.

Taking into account the previous discussion, we define the SINR at reception for the ℓ-th subcarrier as

$$\mathrm{SINR}[\ell] = \frac{|\boldsymbol{h}^{\mathrm{H}}[i]\boldsymbol{F}_{\mathrm{A}}^{0}\boldsymbol{f}_{\mathrm{D}}[\ell]|^2}{\sum_{(q,j)\in\mathcal{H}_i\setminus(0,\ell)}|\boldsymbol{h}^{\mathrm{H}}[i]\boldsymbol{F}_{\mathrm{A}}^{q}\boldsymbol{f}_{\mathrm{D}}[j]|^2+\sigma^2}, \quad (25)$$

where $i=\Delta_f\ell$, and

$$\sum_{(q,j)\in\mathcal{H}_i\setminus(0,\ell)}|\boldsymbol{h}^{\mathrm{H}}[i]\boldsymbol{F}_{\mathrm{A}}^{q}\boldsymbol{f}_{\mathrm{D}}[j]|^2 \quad (26)$$

is the power corresponding to the HI [cf. (13)].

In this work, we establish the average per-subcarrier achievable rate as the system performance metric, that is

$$R=\frac{1}{L}\sum_{\ell=0}^{L-1}\log_2(1+\mathrm{SINR}[\ell]), \quad (27)$$

where $L=\lfloor\frac{N_{\mathrm{c}}}{\Delta_f}\rfloor$ is the effective number of transmitted data symbols within an OFDM symbol. Hence, the hybrid precoders are designed to maximize R subject to a transmit power constraint P_{TX}, leading to the following optimization problem

$$\max_{\{\boldsymbol{F}_{\mathrm{A}}^{q}\}_{q=-\infty}^{\infty},\{\boldsymbol{f}_{\mathrm{D}}[\ell]\}_{\ell=0}^{L-1}} R \quad \text{s.t. } P_{\mathrm{TX}}^{\mathrm{TMA}}\leq P_{\mathrm{TX}}, \quad (28)$$

where $P_{\mathrm{TX}}^{\mathrm{TMA}}$ is that in (20).

An approach to maximize the achievable rate is to maximize the sum SINR over all the effective subcarriers [37]. Therefore, instead of (28) we consider the simpler problem formulation

$$\max_{\{\boldsymbol{F}_{\mathrm{A}}^{q}\}_{q=-\infty}^{\infty},\{\boldsymbol{f}_{\mathrm{D}}[\ell]\}_{\ell=0}^{L-1}} \sum_{\ell=0}^{L-1}\mathrm{SINR}[\ell] \quad \text{s.t. } P_{\mathrm{TX}}^{\mathrm{TMA}}\leq P_{\mathrm{TX}}. \quad (29)$$

Observe that the analog precoding matrices corresponding to all the harmonics are considered in (28) and (29). This is because the SR causes the interference in (25). In addition, it must be considered in the power constraint. However, the harmonic analog precoders $\boldsymbol{F}_{\mathrm{A}}^{q}$ at $q\neq 0$ are coupled through (6) and cannot be independently selected. In addition, the SINR expression (25) critically depends on Δ_f and Δ_t.

In the ensuing sections we will address the design of the proposed SPDT hybrid precoder by solving the optimization problem (28). In Sec. V we focus on the configuration of the OFDM modulation parameters Δ_f and Δ_t. Next, in Sec. VI-A and Sec. VI-B we determine the hybrid precoders for given Δ_f and Δ_t.

V. OFDM MODULATION CONFIGURATION

In this section we propose different settings for the OFDM modulation parameters Δ_f and Δ_t to enable the transmission of wideband OFDM signals using TMAs.

A. REMOVAL OF HARMONIC INTERFERENCE

It is apparent from the SINR expression (25) that, when a TMA is used to transmit over a frequency selective channel, the system performance is limited by the HI in the high SNR regime. In this section, we explain how to select Δ_f and Δ_t to avoid HI.

Zero-Forcing (ZF) is a frequent approach to remove interference in exchange of a reduction in the potential channel gain. Given the particular features of the HI, ZF approaches do not apply. Indeed, note from (25) that the channel response $\boldsymbol{h}[i]$ is the same for both the useful data and the interference. In addition, the design of the precoding matrices $\boldsymbol{F}_{\mathrm{A}}^0$ and $\boldsymbol{F}_{\mathrm{A}}^q$ ($q \neq 0$) are coupled. Then, the spatial features of $\boldsymbol{F}_{\mathrm{A}}^0$ and $\boldsymbol{F}_{\mathrm{A}}^q$ are similar, and the digital precoders $\boldsymbol{f}_{\mathrm{D}}[\ell]$ are unable to provide enough degrees of freedom to cancel the interference.

Alternatively, we consider the different approach of setting adequate values for Δ_f and Δ_t in (8) to remove the HI. In particular, let us consider an analog precoding matrix $\boldsymbol{F}_{\mathrm{A}}(t)$ having K non-negligible harmonics, i.e., $\|\boldsymbol{F}_{\mathrm{A}}^q\|_{\mathrm{F}}^2 \approx 0$ for $|q| > \frac{K-1}{2}$. We demonstrate in Appendix I-A that, by setting $\Delta_f = \frac{K+1}{2}$ and an appropriate value for Δ_t, the HI is removed from the received effective vector symbols $\boldsymbol{x}_u[i]$ in (13). Hence, the signal model reduces to $\boldsymbol{x}_u[i] \approx \boldsymbol{F}_{\mathrm{A}}^0 \boldsymbol{f}_{\mathrm{D}}[\ell] s[\ell]$, and the SINR expression (25) simplifies to

$$\mathrm{SINR}[\ell] \approx \frac{|\boldsymbol{h}^{\mathrm{H}}[\Delta_f \ell] \boldsymbol{F}_{\mathrm{A}}^0 \boldsymbol{f}_{\mathrm{D}}[\ell]|^2}{\sigma^2}. \tag{30}$$

Fig. 3 shows an example of useful symbol using this configuration. As can be appreciated, the harmonic replicas overlap each other but the useful subcarriers containing the data are not affected by any of them. Therefore, we remove the HI introduced by the TMA.

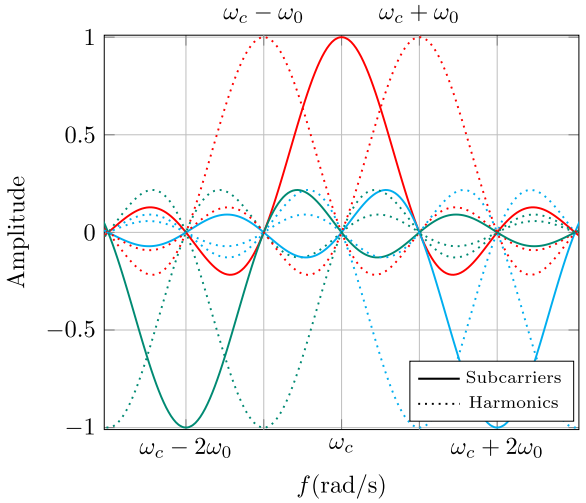

FIGURE 3. Example of effective symbol x_u for $K = 3$, $\Delta_f = 2$, $\Delta_t = 1$, and data symbols $\{-1, 1, -1\}$. The subcarriers for harmonic replicas $\omega_c \pm \omega_0$ overlap whereas data subcarriers ω_c, $\omega_c \pm 2\omega_0$ are free of interference.

A clear advantage of this OFDM symbol configuration is the simpler design of the hybrid precoders, since the choice of Δ_f and Δ_t as in App. I-A reduces to the joint maximization of the SINR in all the subcarriers. The counterpart is that the non-useful subcarriers are totally ignored. In the following subsection we will see a different OFDM symbol configuration suitable to exploit the redundancy available in the non-useful subcarriers.

B. EXPLOITATION OF CHANNEL FREQUENCY DIVERSITY

We seek an OFDM symbol configuration using Q additional subcarriers on the right and other Q subcarriers on the left to transmit each data symbol $s[\ell]$. These subcarriers are consecutive if $\Delta_t = 1$, and separated by Δ_t subcarriers, otherwise. In total, the configuration uses up to $2Q + 1$ subcarriers per data symbol $s[\ell]$, with $2Q+1 \leq K$. Then, the SINR definition of (25) has to be extended to

$$\overline{\mathrm{SINR}}[\ell] = \sum_{q=-Q}^{Q} \frac{|\boldsymbol{h}^{\mathrm{H}}[a(q,\ell)] \boldsymbol{F}_{\mathrm{A}}^q \boldsymbol{f}_{\mathrm{D}}[\ell]|^2}{\sum_{(\nu,\kappa)\in\mathcal{I}_{a(q,\ell)}} |\boldsymbol{h}^{\mathrm{H}}[a(q,\ell)] \boldsymbol{F}_{\mathrm{A}}^{\nu} \boldsymbol{f}_{\mathrm{D}}[\kappa]|^2 + \sigma^2}, \tag{31}$$

where $a(q, \ell) = \Delta_t q + \Delta_f \ell$ is the auxiliary function introduced in (14) and $\mathcal{I}_{a(q,\ell)}$ is the set of replicas that interfere the ℓ-th symbol at subcarrier $a(q, \ell)$, i.e., $\mathcal{I}_{a(q,\ell)} = \mathcal{H}_{a(q,\ell)} \backslash (q, \ell)$, with $\mathcal{H}_{a(q,\ell)}$ given by (14).

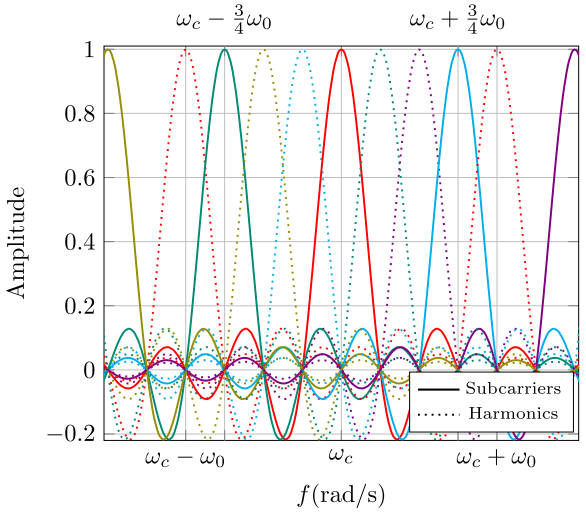

FIGURE 4. Example of effective symbol for $K = 3$, $\Delta_f = 3$, $\Delta_t = 4$, and data symbols $\{1, 1, 1, 1, 1\}$. Both the data and the harmonic replica subcarriers ω_c, $\omega_c \pm \frac{3}{4}\omega_0$, $\omega_c \pm \frac{3}{2}\omega_0$, and $\omega_c \pm \frac{1}{4}\omega_0$, $\omega_c \pm \frac{1}{2}\omega_0$, $\omega_c \pm \omega_0$, $\omega_c \pm \frac{5}{4}\omega_0$, are free of interference.

As in Sec. V-A, appropriate values of Δ_f and Δ_t can be chosen to avoid HI. Assuming that $\Delta_f = K$ and Δ_t are co-prime numbers, we prove in App. I-B that interference is avoided for all the N_c subcarriers. Fig. 4 shows an example of this OFDM configuration for $K = 3$, $\Delta_f = 3$ and $\Delta_t = 4$.

When using the proper choice of Δ_f and Δ_t, the interference set $\mathcal{I}_{a(q,\ell)}$ in (31) only contains the harmonic indices $|\nu| > \frac{K-1}{2}$ and the HI is avoided. Thus, the SINR expression

(31) reduces to

$$\overline{\text{SINR}}[\ell] \approx \sum_{q=-Q}^{Q} \frac{|\boldsymbol{h}^{\text{H}}[a(q,\ell)]\boldsymbol{F}_{\text{A}}^{q}\boldsymbol{f}_{\text{D}}[\ell]|^2}{\sigma^2}. \tag{32}$$

Besides the apparent SINR increase, this approach allows frequency diversity exploitation. In addition, using different subcarriers to detect the same data symbol provides an extra flexibility for TMA hybrid precoding design. However, to fully benefit from frequency diversity, we need to tackle the limitations arising when using TMAs to implement analog precoding.

In Sec. V-A, the integer factors Δ_f and Δ_t were chosen to remove the HI in the fundamental mode. Contrarily, in this section we consider several harmonic replicas of the same data symbol, but still avoiding HI. In some scenarios, however, it might be interesting to explore mixed strategies. For instance, consider the case where some of the harmonic replicas present reduced power but cannot be disregarded. A mixed approach in this context might exploit the subset of harmonic replicas having the largest power, allowing overlapping in the remaining ones.

VI. HYBRID PRECODING DESIGNS

In the following, we propose two TMA hybrid precoder designs considering the symbol configurations of Sec. V, and their respective effects over the HI.

A. HYBRID PRECODING WITHOUT DIVERSITY

In this section we focus on the OFDM symbol configuration of Sec. V-A, that exploits the subcarriers corresponding to $q = 0$ and ignores the remaining ones. In the analog domain, we first design the precoding matrix $\boldsymbol{F}_{\text{A}}^{0}$. Considering the analog precoding matrices for all q at this point makes the optimization problem (29) extremely difficult. Therefore, substituting (30) into (29) leads to

$$\max_{\boldsymbol{F}_{\text{A}}^{0}\in\mathcal{F},\{\boldsymbol{f}_{\text{D}}[\ell]\}_{\ell=0}^{L-1}} \sum_{\ell=0}^{L-1} \frac{|\boldsymbol{h}^{\text{H}}[\Delta_f\ell]\boldsymbol{F}_{\text{A}}^{0}\boldsymbol{f}_{\text{D}}[\ell]|^2}{\sigma^2} \quad \text{s.t. } P_{\text{TX}}^{\text{TMA}} \le P_{\text{TX}}. \tag{33}$$

Although the former optimization problem neglects the SR, $q \neq 0$, this issue will be addressed next in Sec. VI-A1.

In the digital domain, the baseband precoder $\boldsymbol{f}_{\text{D}}[\ell]$ for the useful subcarrier ℓ can be decomposed as $\boldsymbol{f}_{\text{D}}[\ell] = \tilde{\boldsymbol{f}}_{\text{D}}[\ell]p[\ell]$, where $p[\ell]$ is the power allocation and $\tilde{\boldsymbol{f}}_{\text{D}}[\ell]$ is the precoding direction. For a given analog precoder $\boldsymbol{F}_{\text{A}}^{0}$, the baseband precoding direction that maximizes the SINR in (30) is

$$\tilde{\boldsymbol{f}}_{\text{D}}[\ell] = \frac{\boldsymbol{F}_{\text{A}}^{0,\text{T}}\boldsymbol{h}[\Delta_f\ell]}{\|\boldsymbol{F}_{\text{A}}^{0}\boldsymbol{F}_{\text{A}}^{0,\text{T}}\boldsymbol{h}[\Delta_f\ell]\|_2}, \tag{34}$$

where the normalization ensures $\|\boldsymbol{F}_{\text{A}}^{0}\tilde{\boldsymbol{f}}_{\text{D}}[\ell]\|_2^2 = 1$.

It is also possible to obtain a closed form expression for the analog precoders that maximizing the sum SINR. To that end, we define the equivalent channels

$$h_{eq}[\ell] = \boldsymbol{h}^{\text{H}}[\Delta_f\ell]\boldsymbol{F}_{\text{A}}^{0}\tilde{\boldsymbol{f}}_{\text{D}}[\ell], \tag{35}$$

and maximize the sum of their corresponding gains $\sum_{\ell=0}^{L}|h_{eq}[\ell]|^2$.

Let us introduce the wideband channel matrix, $\boldsymbol{H}$, containing the channel responses for the L useful subcarriers

$$\boldsymbol{H} = \left[\boldsymbol{h}^{*}[0], \boldsymbol{h}^{*}[\Delta_f], \ldots, \boldsymbol{h}^{*}[\Delta_f(L-1)]\right]^{\text{T}}. \tag{36}$$

Now, by using $\tilde{\boldsymbol{f}}_{\text{D}}[\ell]$ in (34), the sum gain reads as

$$\begin{aligned}\sum_{\ell=0}^{L-1}|h_{eq}[\ell]|^2 &= \sum_{\ell=0}^{L-1}\frac{|\boldsymbol{h}^{\text{H}}[\Delta_f\ell]\boldsymbol{F}_{\text{A}}^{0}\boldsymbol{F}_{\text{A}}^{0,\text{T}}\boldsymbol{h}[\Delta_f\ell]|^2}{\|\boldsymbol{F}_{\text{A}}^{0}\boldsymbol{F}_{\text{A}}^{0,\text{T}}\boldsymbol{h}[\Delta_f\ell]\|_2^2}\\ &= \text{tr}\left(\boldsymbol{F}_{\text{A}}^{0,\text{T}}\sum_{\ell=0}^{L-1}\boldsymbol{h}[\Delta_f\ell]\boldsymbol{h}^{\text{H}}[\Delta_f\ell]\boldsymbol{F}_{\text{A}}^{0}\right)\\ &= \|\boldsymbol{H}\boldsymbol{F}_{\text{A}}^{0}\|_{\text{F}}^2\end{aligned}$$

where we used the fact that $\boldsymbol{F}_{\text{A}}^{0}$ is a semi-unitary matrix. Then, maximizing the sum of the equivalent channel gains is the same as maximizing $\|\boldsymbol{H}\boldsymbol{F}_{\text{A}}^{0}\|_{\text{F}}^2$. Correspondingly, $\boldsymbol{F}_{\text{A}}^{0}$ is readily determined as

$$\begin{aligned}\boldsymbol{F}_{\text{A}}^{0} &= \underset{\boldsymbol{F}\in\mathcal{F}}{\text{argmax}}\,\|\boldsymbol{H}\boldsymbol{F}\|_{\text{F}}^2 \quad \text{s.t. } \|\boldsymbol{F}\|_{\text{F}}^2 = N_{\text{RF}}\\ &= \underset{\boldsymbol{F}\in\mathcal{F}}{\text{argmax}}\,\text{tr}\left(\boldsymbol{F}^{\text{T}}\Re\{\boldsymbol{H}^{\text{H}}\boldsymbol{H}\}\boldsymbol{F}\right) \quad \text{s.t. } \|\boldsymbol{F}\|_{\text{F}}^2 = N_{\text{RF}},\end{aligned} \tag{37}$$

where $\Re\{\boldsymbol{X}\}$ and $\Im\{\boldsymbol{X}\}$ represent the real and imaginary parts of a complex matrix $\boldsymbol{X}$, respectively, and we used that $\text{tr}(\boldsymbol{F}^{\text{T}}\Im\{\boldsymbol{H}^{\text{H}}\boldsymbol{H}\}\boldsymbol{F}) = 0$. The analog precoder is then computed as $\boldsymbol{F}_{\text{A}}^{0} = \boldsymbol{U}$, where $\boldsymbol{U}$ comprises the eigenvectors associated to the N_{RF} largest eigenvalues of $\Re\{\boldsymbol{H}^{\text{H}}\boldsymbol{H}\}$. Note that this design is optimal to (37).

1) REDUCING THE SIDEBAND RADIATION

Thus far, precoders in the analog domain have been designed without taking into account the SR. Reducing the SR is beneficial because it improves the TMA power efficiency given by (21) and leads to a smaller number of significant harmonics K which allows to reduce Δ_f.

It is clear from (1) that normalized pulse durations $\xi_{m,r}$ close to 0 or 1 lead to similar values $|[\boldsymbol{F}_{\text{A}}^{0}]_{m,r}| \approx 1$, $\forall m$ and waste small amounts of power over the harmonic frequencies. Conversely, analog precoding matrices satisfying this condition would lead to smaller equivalent channel gains. That is, there is a tradeoff between these two features. Therefore, in order to reduce the SR, we propose to follow the strategy in [23] where the columns of the target analog precoder, $\boldsymbol{f}_{\text{A},r}^{0} = [\boldsymbol{F}_{\text{A}}^{0}]_{:,r}$, are updated to reduce the difference between the largest and the smallest absolute value of their entries. To that end, we introduce the problem formulation

$$\boldsymbol{g}_{\text{A},r}^{0} = \underset{\boldsymbol{g}}{\text{argmax}}\,\boldsymbol{g}^{\text{T}}\boldsymbol{f}_{\text{A},r}^{0} + \gamma(\min_{m}[\boldsymbol{g}]_m - \max_{n}[\boldsymbol{g}]_n), \tag{38}$$

where $\boldsymbol{g}_{\text{A},r}^{0}$ is the r-th analog precoding column with reduced SR. Note that (38) contains a penalization term weighted by γ. This parameter should be set according to the strength of the undesired radiation generated by the TMA. The solution

to (38) in [23] is obtained with a convex solver. Here, we propose to solve (38) using a steepest descent method. Thus, each step updates the analog precoding vector as

$$\boldsymbol{g}_{\mathrm{A},r}^{0,(n+1)} = \boldsymbol{g}_{\mathrm{A},r}^{0,(n)} + \mu\left(\boldsymbol{f}_{\mathrm{A},r}^{0} + \gamma(\boldsymbol{e}_m - \boldsymbol{e}_n)\right), \tag{39}$$

where μ is the step size and $\boldsymbol{e}_j$ is the vector with zeros except for the j-th entry. Compared to the approach in [23], the computational complexity of the former update is negligible.

Accordingly, the analog precoding matrix $\boldsymbol{G}_{\mathrm{A}}^{0}$ contains the columns $\boldsymbol{g}_{\mathrm{A},r}^{0}$, $r = 1, \ldots, N_{\mathrm{RF}}$. The baseband precoder direction of (34) uses $\boldsymbol{G}_{\mathrm{A}}^{0}$ as the analog precoding matrix. In addition, we also use $\boldsymbol{G}_{\mathrm{A}}^{0}$ to compute the equivalent gains $|h_{eq}[\ell]|^2$ of (35). Next, we use these gains to determine the power allocation $p[\ell]$ satisfying $P_{\mathrm{TX}}^{\mathrm{TMA}} \leq P_{\mathrm{TX}}$ via waterfilling. Eventually, the hybrid precoder for the ℓ-th subcarrier is given by

$$\boldsymbol{F}_{\mathrm{H}}^{0}[\ell] = \boldsymbol{G}_{\mathrm{A}}^{0}\tilde{\boldsymbol{f}}_{\mathrm{D}}[\ell]p[\ell]. \tag{40}$$

B. HYBRID PRECODING WITH DIVERSITY

We now consider the OFDM symbol configuration in Sec. V-B and address hybrid precoding to exploit the harmonics $|q| \leq Q$. Recall that the proposed TMA precoder sends replicas of the data symbols over the harmonic frequencies. Thus, we take advantage of the most significant $|q| \leq Q$ harmonics by combining them at reception. This way it is possible to exploit the channel frequency diversity and improve performance.

Another advantage of the OFDM symbol configuration in Sec. V-B is the improved TMA power efficiency, since the useful radiated power contains the power radiated over the fundamental mode and the $2Q$ harmonics. Accordingly, the TMA power efficiency reads as

$$\eta^{\mathrm{TMA}} = \frac{\sum_{\ell=0}^{L-1}\sum_{q=-Q}^{Q}\|\boldsymbol{F}_{\mathrm{A}}^{q}\boldsymbol{f}_{\mathrm{D}}[\ell]\|_{\mathrm{F}}^{2}}{P_{\mathrm{TX}}^{\mathrm{TMA}}}. \tag{41}$$

If the harmonics $-Q \leq q \leq Q$ hold most of the radiated power, only a small portion is not profitably used.

As explained in Sec. V-B, when appropriately selecting Δ_f and Δ_t, the SINR at reception for subcarrier ℓ is given by (32). Thus, the optimization problem (29) becomes

$$\begin{aligned}\max_{\{\boldsymbol{F}_{\mathrm{A}}^{q}\}_{q=-Q}^{Q},\{\boldsymbol{f}_{\mathrm{D}}[\ell]\}_{\ell=0}^{L-1}} & \sum_{\ell=0}^{L-1}\sum_{q=-Q}^{Q}\frac{|\boldsymbol{h}^{\mathrm{H}}[a(q,\ell)]\boldsymbol{F}_{\mathrm{A}}^{q}\boldsymbol{f}_{\mathrm{D}}[\ell]|^2}{\sigma^2}\\ \text{s.t. } & P_{\mathrm{TX}}^{\mathrm{TMA}} \leq P_{\mathrm{TX}}.\end{aligned} \tag{42}$$

Notice that considering more harmonic frequencies into the useful power does not necessarily imply the improvement of the performance metric. Under this approach, the wideband channel matrix $\boldsymbol{H}$ contains the channel responses

$$\begin{aligned}\boldsymbol{H} = \big[&\boldsymbol{h}^{*}[0], \boldsymbol{h}^{*}[\Delta_t], \ldots, \boldsymbol{h}^{*}[Q], \boldsymbol{h}^{*}[-Q+\Delta_f], \ldots,\\ &\boldsymbol{h}^{*}[Q+\Delta_f], \ldots, \boldsymbol{h}^{*}[Q+\Delta_f(L+1)]\big]^{\mathrm{T}},\end{aligned} \tag{43}$$

where we avoid frequency index repetitions. As a consequence, for the harmonic frequencies $|q| \leq Q$, we obtain the equivalent channel gain

$$h_{eq}[\ell] = \sum_{q=-Q}^{Q}|\boldsymbol{h}^{\mathrm{H}}[a(q,\ell)]\boldsymbol{F}_{\mathrm{A}}^{q}\tilde{\boldsymbol{f}}_{\mathrm{D}}[\ell]|^2 \tag{44}$$

for the ℓ-th data symbol.

Due to the relationship in (1), designing the analog precoder for $\boldsymbol{F}_{\mathrm{A}}^{0}$ also determines $\boldsymbol{F}_{\mathrm{A}}^{q}$, $q \neq 0$. However, the spatial signature of the analog precoding matrices corresponding to the replicas vary from that of $\boldsymbol{F}_{\mathrm{A}}^{0}$. Thereby, the equivalent channel gains are small for $\boldsymbol{F}_{\mathrm{A}}^{q}$ with $q \neq 0$.

1) ANALOG PRECODING MATRICES

To achieve a good performance it is desirable to have similar gains in all the useful harmonics. This can be accomplished by keeping the spatial structure of $\boldsymbol{F}_{\mathrm{A}}^{q}$ similar to that of $\boldsymbol{F}_{\mathrm{A}}^{0}$ for $|q| \leq Q$. That is, $\boldsymbol{F}_{\mathrm{A}}^{q} \approx \boldsymbol{F}_{\mathrm{A}}^{0}\boldsymbol{D}^{q}$ where $\boldsymbol{D}^{q} = \mathrm{diag}\{d_1^q, d_2^q, \ldots, d_{N_{\mathrm{RF}}}^q\}$ is a diagonal matrix. Decomposing this matrix condition column-wise, we obtain the following set of vector conditions

$$\boldsymbol{f}_{\mathrm{A},r}^{0} \approx d_r^q\boldsymbol{f}_{\mathrm{A},r}^{q}, \quad r = 1, \ldots, N_{\mathrm{RF}},\ q = -Q, \ldots, Q \tag{45}$$

where $\boldsymbol{f}_{\mathrm{A},r}^{0}$ and $\boldsymbol{f}_{\mathrm{A},r}^{q}$ are the r-th column of $\boldsymbol{F}_{\mathrm{A}}^{0}$ and $\boldsymbol{F}_{\mathrm{A}}^{q}$, respectively. Nevertheless, the coupling in (1) makes this task extremely difficult.

A feasible strategy to achieve the condition in (45) is setting the analog precoding vector as $|\boldsymbol{g}_{\mathrm{A},r}^{0}| \approx a\boldsymbol{1}$, for some scalar parameter a. This strategy can be formalized through the following convex optimization problem

$$\begin{aligned}\boldsymbol{g}_{\mathrm{A},r}^{0} = \underset{\boldsymbol{g}\in\mathbb{R}^M, t\geq 0}{\mathrm{argmax}}\ & t - \beta\|\boldsymbol{g}\|_2\\ \text{s.t. } & |\boldsymbol{g}^{\mathrm{T}}\boldsymbol{f}_{\mathrm{A},r}^{0}| = t\\ & \|\boldsymbol{g}\|_\infty \leq a\end{aligned} \tag{46}$$

where $\boldsymbol{f}_{\mathrm{A},r}^{0}$ is the r-th column of the real precoding direction obtained by solving (37) with $\boldsymbol{H}$ in (43) and $h_{eq}[\ell]$ in (44). Large values of the penalty parameter $\beta \geq 0$ lead to scaled versions of the desired direction, $\boldsymbol{g}_{\mathrm{A},r}^{0} \approx c\boldsymbol{f}_{\mathrm{A},r}^{0}$, for some c. Contrarily, reducing β increases the number of vector entries set to a, yielding $|\boldsymbol{g}_{\mathrm{A},r}^{0}| \approx a\boldsymbol{1}$. The choice of β strongly depends on the number of significant harmonics K.

Compared to the solution where $\|\boldsymbol{g}\|_\infty \leq a$ is not imposed, this approach incurs a reduction on the equivalent channel gain for the fundamental mode. Therefore, the resulting analog precoder design achieves a trade-off between the equivalent channel gain for $q = 0$ and the diversity gain. In the interest of proving further insight, we consider the normalized precoding vector $\|\boldsymbol{g}\|_2 = 1$. Then, the equivalent channel gain loss for $q = 0$ lies on the interval

$$\frac{1}{M}\|\boldsymbol{f}_{\mathrm{A},r}^{0}\|_1^2 \leq |\boldsymbol{g}_{\mathrm{A},r}^{0,\mathrm{T}}\boldsymbol{f}_{\mathrm{A},r}^{0}| \leq \|\boldsymbol{f}_{\mathrm{A},r}^{0}\|_2^2 = 1. \tag{47}$$

Note that equality holds when the signal impinges the center of the antenna array, i.e., for $\vartheta_l = 0$ and $N_{\mathrm{p}} = 1$ in (15). Therefore, we can conclude that for Line-of-Sight (LoS) scenarios with a dominant channel path and antenna arrays

properly oriented, the use of this approach does not result in a reduction of the equivalent channel gain for $q = 0$. These conditions are reasonable for, e.g., indoor scenarios.

The flexibility to organize the harmonics offered by the OFDM symbol configuration in Sec. V-B is key to achieve the desired frequency diversity at the receiver side. This flexibility is not possible in conventional TMAs (e.g. [15], [16], [38]) where the power distribution among the harmonic modes quickly reduces with q, i.e., $\|\boldsymbol{F}_{\mathrm{A}}^{|q|}\|_{\mathrm{F}} \geq \|\boldsymbol{F}_{\mathrm{A}}^{|q+1|}\|_{\mathrm{F}} \, \forall q$.

On the contrary, this situation does not occur in the proposed SPDT TMA analog network. Recall that our goal is to achieve frequency diversity and reasonable equivalent channel gains for the $2Q + 1$ useful harmonics. Therefore, we determine the value of the parameter a according to this strategy. That is, we determine a pulse duration ξ such that the transmit power is evenly distributed among a number of useful harmonics. For example, it is possible to get the first three harmonic frequencies, $q = -1, 0, 1$ to have equal transmit power by finding ξ such that

$$2\xi \, \mathrm{sinc}(\pi\xi) = 2\xi - 1. \tag{48}$$

Last equality yields $\xi = 0.735$ or $\xi = 0.265$ and $\varrho = \frac{-T_0}{2}$. Moreover, for the useful harmonics selections $|q| \leq 1$ and $|q| \leq 2$, the power efficiencies are $\eta^{\mathrm{TMA}} \approx 0.7$ and $\eta^{\mathrm{TMA}} \approx 0.9$, respectively. Accordingly, we set $a = 2\xi - 1$ in (46) and gather the solutions for each column $r = \{1, \ldots, N_{\mathrm{RF}}\}$ to obtain the analog precoder $\boldsymbol{G}_{\mathrm{A}}^{0}$.

2) BASEBAND PRECODING DESIGN

Considering the OFDM symbol configuration in Sec. V-B and a small value of β in (46), we get that the analog precoding matrices meet the condition $\boldsymbol{F}_{\mathrm{A}}^{q} \approx \boldsymbol{F}_{\mathrm{A}}^{0} d^{q}$. Thus, the SINR in (32) can be rewritten as

$$\overline{\mathrm{SINR}}[\ell] \approx \frac{\boldsymbol{f}_{\mathrm{D}}^{\mathrm{H}}[\ell]\boldsymbol{F}_{\mathrm{A}}^{0,\mathrm{T}}\boldsymbol{W}[\ell]\boldsymbol{F}_{\mathrm{A}}^{0}\boldsymbol{f}_{\mathrm{D}}[\ell]}{\sigma^2}, \tag{49}$$

with $\boldsymbol{W}[\ell] = \sum_{q=-Q}^{Q} (d^q)^2 \boldsymbol{h}[a(q,\ell)]\boldsymbol{h}^{\mathrm{H}}[a(q,\ell)]$. Furthermore, the total transmit power (20) simplifies to $P_{\mathrm{TX}}^{\mathrm{TMA}} = \sum_{q=-\infty}^{\infty} (d^q)^2 \sum_{\ell=0}^{L-1} \|\boldsymbol{F}_{\mathrm{A}}^{0}\boldsymbol{f}_{\mathrm{D}}[\ell]\|_2^2$. From (49), the baseband precoding direction is

$$\tilde{\boldsymbol{f}}_{\mathrm{D}}[\ell] = \frac{\boldsymbol{u}_{\max}[\ell]}{\|\boldsymbol{F}_{\mathrm{A}}^{0}\boldsymbol{u}_{\max}[\ell]\|_2 \sqrt{\sum_{q=-Q}^{Q} (d^q)^2}}, \tag{50}$$

where $\boldsymbol{u}_{\max}[\ell]$ is the principal eigenvector of $\boldsymbol{F}_{\mathrm{A}}^{0,\mathrm{T}}\boldsymbol{W}[\ell]\boldsymbol{F}_{\mathrm{A}}^{0}$. Note that the baseband precoder takes into account the channel responses for the harmonic replicas associated to the data symbol $s[\ell]$. Using the analog precoding matrices $\boldsymbol{G}_{\mathrm{A}}^{0}$ from previous section and $\tilde{\boldsymbol{f}}_{\mathrm{D}}[\ell]$ in (50) we compute the equivalent channel gains of (44). Next, we determine the power allocation $p[\ell]$ via waterfilling. Finally, we obtain the hybrid precoders

$$\boldsymbol{F}_{\mathrm{H}}^{q}[\ell] = \boldsymbol{G}_{\mathrm{A}}^{q}\tilde{\boldsymbol{f}}_{\mathrm{D}}[\ell]p[\ell]. \tag{51}$$

Algorithm 1 summarizes the steps to determine the hybrid precoders in Sec. VI-A and Sec. VI-B.

Algorithm 1 Hybrid Precoding in Sec. VI-A and Sec. VI-B

1: $\boldsymbol{H} \leftarrow$ Collect channel matrices, (36) or (43)
2: $\boldsymbol{F}_{\mathrm{A}}^{0} \leftarrow$ solve (37) for $\boldsymbol{H}$
3: $\boldsymbol{g}_{\mathrm{A},r}^{0} \leftarrow$ solve (38) or (46) with $\boldsymbol{f}_{\mathrm{A},r}^{0}, \forall r \in \{1, \ldots, N_{\mathrm{RF}}\}$
4: $\boldsymbol{G}_{\mathrm{A}}^{0} \leftarrow [\boldsymbol{g}_{\mathrm{A},r}^{0}, \ldots, \boldsymbol{g}_{\mathrm{A},N_{\mathrm{RF}}}^{0}]$
5: $h_{eq}[\ell] \leftarrow$ compute with (35) or (44), $\forall \ell \in \{0, \ldots, L-1\}$
6: $p[\ell] \leftarrow$ compute using waterfilling
7: Determine hybrid precoders with (40) or (51)

VII. NUMERICAL RESULTS

In this section we evaluate empirically the performance of the proposed TMA hybrid precoding approach for wideband OFDM transmissions and analyze the impact of different parameter configurations.

We consider a setup with $M = 64$ transmit antennas, $N_{\mathrm{RF}} = 8$ RF chains, $N_{\mathrm{c}} = 512$ OFDM subcarriers, $f_c = 28$ GHz carrier frequency, and $B_{\mathrm{OFDM}} = 2$ GHz. We generate 500 channel realizations according to the channel model in Sec. III-A with $N_{\mathrm{p}} = 8$ channel paths, random angles ϑ_l uniformly distributed in $[0, \pi]$, and $D = 8$ random delays z_l uniformly distributed in $[0, D-1]T_s$. We assume that the integer factors N and Δ_t are chosen such that the subcarrier separation is adapted to the channel coherence bandwidth. Table 2 shows the simulation parameters in all the numerical experiments unless in the cases explicitly stated.

TABLE 2. Simulation parameters.

Parameter	Value
Number of antennas	$M = 64$
Number of RF chains	$N_{\mathrm{RF}} = 8$
Number of channel paths	$N_{\mathrm{p}} = 8$
Number of OFDM subcarriers	$N_{\mathrm{c}} = 512$
Number of Delay taps	$D = 8$
Carrier frequency	$f_c = 28$ GHz
Signal bandwidth	$B_{\mathrm{OFDM}} = 2$ GHz
Channel gain	$\alpha_l \sim \mathcal{N}_{\mathbb{C}}(0, 1)$
Delay interval	$z_l \in [0, (D-1)T_s]$
AoD interval	$\vartheta_l \in [0, \pi]$
Number of channel realizations	500
Number of significant harmonics	$K = 7$
Penalty parameter in (46)	$\beta = 0$
Penalty parameter in (38)	$\gamma = 2$
Signal-to-Noise Ratio	$\mathrm{SNR} = \frac{P_{\mathrm{TOT}}}{\Delta_f \sigma^2}$
4-bit PS IL	5 dB
TMA IL	0.5 dB

A. PARAMETER CHOICE IN OPTIMIZATION PROBLEMS

Our first experiment aims at determining the parameter β in the optimization problem (46) for $\xi = 0.735$ and $\boldsymbol{f}_{\mathrm{A},r}^{0} = \Re\{\boldsymbol{h}\}$, where $\boldsymbol{h}$ is a random frequency flat channel realization according to (17) with the parameters of Table 2. Remember that the proposed precoded schemes exploit the common channel spatial structure for different frequencies [6].

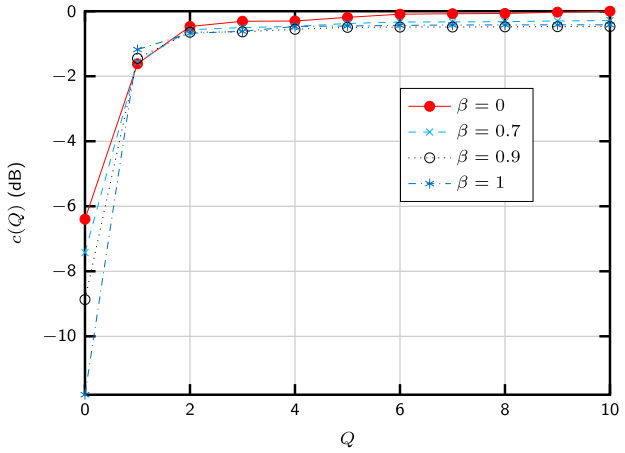

FIGURE 5. Cumulative normalized equivalent channel gains (dB) vs. number of considered harmonic replicas for different values of β in (46). The remaining setup parameters are provided in Table 2.

Then, we use $\boldsymbol{h}[0] = \boldsymbol{h}[1] = \ldots = \boldsymbol{h}[N_c]$ as an extreme case of spatial similarity among different subcarriers to obtain a simpler interpretation of the numerical results. Recall that the value of β represents the tradeoff between an accurate analog precoding vector and a more even power distribution among the first harmonic replicas. Fig. 5 shows the cumulative equivalent channel gain

$$c(Q) = \frac{1}{\rho} \sum_{q=-Q}^{Q} \|\boldsymbol{h}^{\mathrm{H}} \boldsymbol{g}_{\mathrm{A},r}^{q}\|_2^2, \tag{52}$$

for different values of β and ρ is the maximum value of $\sum_{q=-10}^{10} \|\boldsymbol{h}^{\mathrm{H}} \boldsymbol{g}_{\mathrm{A},r}^{q}\|_2^2$ achieved for any β.

As expected, $\beta = 0$ achieves the best equilibrium among the first harmonic replicas since the cumulative gain shows the smoothest increase. Contrarily, if $\beta = 1$ the cumulative gain sharply rises for $q = 1$, indicating that most of the power is concentrated on the harmonics $q = \pm 1$. We also observe that the gain over the fundamental mode $q = 0$ is larger than for $\beta = 0$. Taking into account the losses in (47) this result seems contradictory. Notice however, that the total power constraint over all the harmonic replicas is equal for the different values of β. Thus, when $\beta = 1$ the power radiated over $q = 0$ is very small. Combining these ideas, it is clear that the equivalent channel gain for $q = 0$ is larger when $\beta = 0$, despite the lack of flexibility to design the precoder in this case.

Another advantage of $\beta = 0$ is that obtaining the analog precoding vectors is computationally very efficient, since it only depends on the sign of the entries of the desired precoding direction, i.e., $\boldsymbol{g}_{\mathrm{A},r}^{0} = \mathrm{sign}(\boldsymbol{f}_{\mathrm{A},r}^{0})(2\xi - 1)$. Since the problem formulation of (46) is intended to improve the frequency diversity, we will use $\beta = 0$ in the ensuing computer experiments.

In order to reduce the SR effect in the OFDM configuration of Sec. V-A, we use the optimization problem (38) with $\gamma = 2$.

B. PERFORMANCE EVALUATION

Taking into account the previous results, we set the maximum number of significant harmonics to $K = 7$. Fig. 6 and Fig. 7 plot the average achievable rate given by (27) versus $\mathrm{SNR} = \frac{P_{\mathrm{TOT}}}{\Delta_f \sigma^2}$, where the factor Δ_f ensures that the per-subcarrier SNR is equal for different OFDM symbol configurations. We evaluate several parameter values for both OFDM configurations of Sec. V-A and Sec. V-B, respectively, and their corresponding hybrid precoder designs of Sec. VI-A and Sec. VI-B.

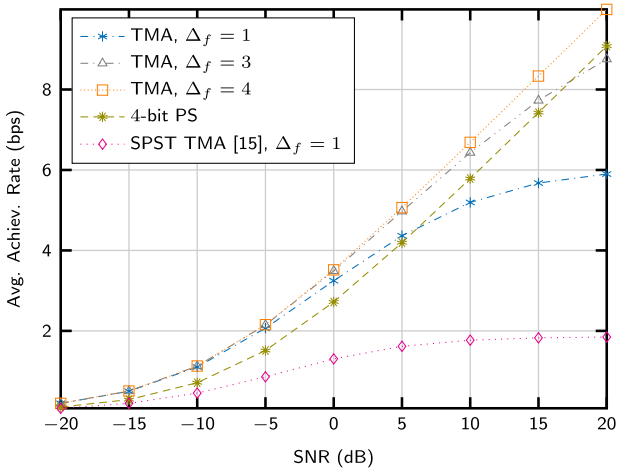

FIGURE 6. Achievable rate (bps) vs. SNR (dB) for $\Delta_f = \{1, 3, 4\}$, the symbol configuration in Sec. V-A, and hybrid precoder in Sec. VI-A. Same symbol configuration and hybrid precoders are evaluated with SPST-based analog network of [15]. The setup parameters are provided in Table 2.

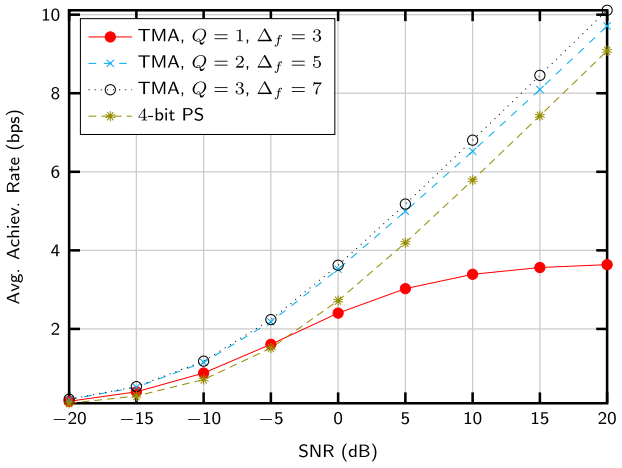

FIGURE 7. Achievable rate (bps) vs. SNR (dB) for $Q = \{1, 2, 3\}$, $\Delta_f = \{3, 5, 7\}$, the symbol configuration in Sec. V-B and hybrid precoder in Sec. VI-B. The setup parameters are provided in Table 2.

Fig. 6 and Fig. 7 also plot the results obtained with a phased array analog precoder (see Fig. 2). Following the analysis of Sec. IV-A, all precoders consume the same total power available, P_{TOT}, while the corresponding ILs associated to the PSs and TMA inefficiencies are taken into account in each precoding scheme. Recall that the efficiency of a TMA is

larger in practice, since the effects associated to the additional PAs necessary to compensate the ILs of the PSs are not considered in our experiments.

As observed in Fig. 6, the parameter Δ_f has a large impact on the achievable rate. In particular, the interference introduced by the harmonic replicas is tightly related to this parameter. As a consequence, maximizing the SNR and neglecting the HI is useful for environments with low SNR, where the proposed TMA precoder with $\Delta_f = 1$ performs better than phased array precoding with PSs. For instance, this is the case of Non Line-of-sight (NLOS) mmWave scenarios where the SNRs are moderate to low due to the high propagation losses [2]. Moreover, for SNR $\leq$ 5 dB, the proposed TMA precoder gets in all cases a performance better than the PS precoder. For SNRs larger than 5 dB and $\Delta_f = 1$, the HI limits the performance and the achievable rate saturates. Indeed, this metric clearly illustrates the impact of HI on performance, since it gradually reduces for decreasing Δ_f and high SNR values. Furthermore, when $\Delta_f = 4$, the HI is completely removed and we achieve the best performance for the whole SNR regime. Finally, we include the SPST analog network of [15]. Besides HI, we consider a 1dB IL for the 1-bit PS required in this scheme, as well as the losses associated to the power absorption during the SPST switches off-state. Such losses are the main source of power inefficiency, leading to poor performance results.

Fig. 7 shows the achievable rate versus SNR for the OFDM symbol configuration of Sec. V-B. Recall that we are considering $K = 7$ significant harmonics. Accordingly, we set $Q \leq 3$ as the number of useful harmonics. Under this assumption, we performed simulations for different values of Δ_f, using $\beta = 0$ for the determination of the TMA hybrid precoders.

Fig. 7 shows how the successful exploitation of the channel frequency diversity allows to achieve a good performance using the proposed SPDT TMA precoder. Clearly, using a small frequency separation, i.e. $\Delta_f = 3$, is not a good choice since it leads to a strong HI. In contrast, using larger separations, like $\Delta_f = 5$ or $\Delta_f = 7$ (which ensures a total absence of HI for all the harmonic replicas), provides better results. Recall that the equivalent channel gains obtained with the configuration in Sec. V-B are smaller compared to those achieved with the configuration of Sec. V-A. Therefore, the larger power efficiency and increased frequency diversity compensate the smaller array gain, but the performance gain is not outstanding compared to the results in Fig. 6.

Let us introduce the power efficiency as the ratio between the useful power (which depends on the symbol configuration, analog precoder, and analog network implementation), and the total power P_{TOT} in (22) common to all the schemes. We now compare this power efficiency for the schemes evaluated in Fig. 6 and Fig. 7, for the setup parameters in Table 2. In particular, for the symbol configuration in Sec. V-A, and hybrid precoder in Sec. VI-A we only show the configuration $\Delta_f = 4$, as the symbols configurations for $\Delta_f = 1$ and $\Delta_f = 3$ exhibit the same efficiency value, around 0.7.

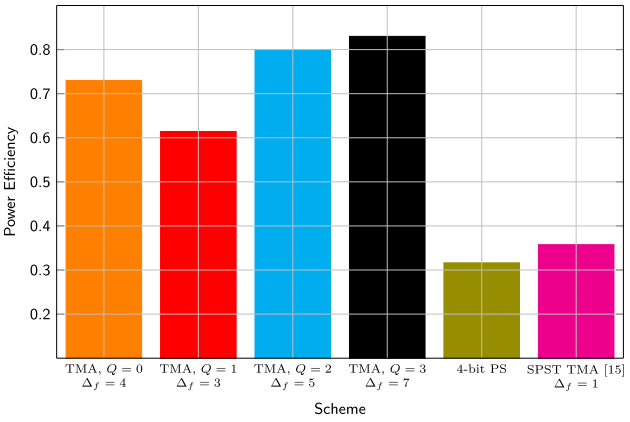

FIGURE 8. Power efficiency vs. Scheme for $\Delta_f = 4$ and the symbol configuration in Sec. V-A, and for $Q = \{1, 2, 3\}$, $\Delta_f = \{3, 5, 7\}$ and the symbol configuration in Sec. V-B. $\Delta_f = 1$ and the symbol configuration in Sec. V-A are employed for the SPST-based analog network of [15]. The setup parameters are provided in Table 2.

Moreover, we see the power wasted when the analog network is built using SPST switches, leading to an efficiency value below 0.4. For the symbol configuration in Sec. V-B and hybrid precoder in Sec. VI-B we consider several parameter settings, $Q = \{1, 2, 3\}$ with $\Delta_f = \{3, 5, 7\}$. As expected, the power efficiency increases with the number of useful harmonics and this configuration reaches the largest efficiencies, with values over 0.8 for $Q = 3$ and $\Delta_f = 7$. We also show results for the analog network employing 4-bit PSs. Again, the power efficiency is improvable, as it only reaches a modest value of 0.3. As shown in Table 1, the power efficiency depends on the number of transmit antennas. Since we consider a relatively small number of antennas, $M = 64$, we would observe that the efficiency gap of TMA implementations with respect to the PS-based solutions would increase for larger values of M.

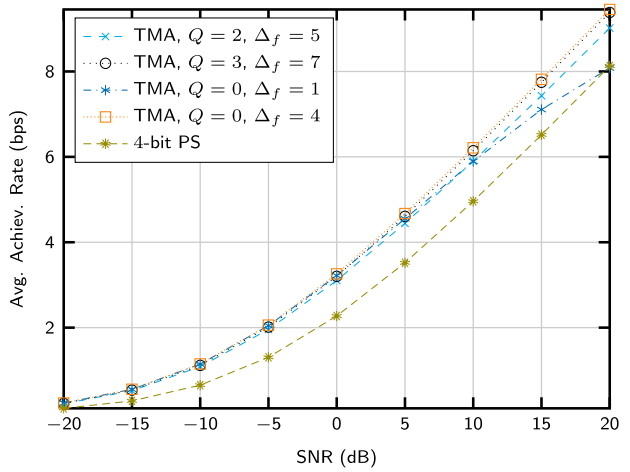

FIGURE 9. Achievable rate (bps) vs. SNR (dB) for $\Delta_f = \{1, 4\}$ and the symbol configuration in Sec. V-A, and for $Q = \{2, 3\}$, $\Delta_f = \{5, 7\}$ and the symbol configuration in Sec. V-B. The number of paths is $N_p = 1$ and $\vartheta \in [-\frac{\pi}{6}, \frac{\pi}{6}]$.

Fig. 9 shows results for a LoS scenario where the dominant path impinges close to the center of the array. To simulate

these scenarios, we set $N_{\mathrm{p}} = 1$ and consider uniformly distributed random angles ϑ within the interval $[-\frac{\pi}{6}, \frac{\pi}{6}]$, corresponding to a sector of 60°. This setting properly models certain practical situations where the antenna arrays focus on one or a few propagation paths like, e.g., indoor or small cell mmWave environments. As shown in Sec. VI-B1, the equivalent channel gains achieved using the analog precoders with $\beta = 0$ are near optimal [cf. (47)]. Observe that, for $\vartheta = 0$, the entries in the steering vector of (16) are real valued and TMA real precoders achieve the channel gains of digital precoding. Further, this feature approximately holds for $\vartheta \in [-\frac{\pi}{6}, \frac{\pi}{6}]$. Therefore, Sec. V-A and Sec. V-B OFDM symbol configurations exhibit a remarkably good performance in this setting. For example, for $Q = 0$ and $\Delta_f = 1$, the proposed TMA approach provides a substantial performance gain with respect to the PS-based analog precoder, with similar results for 20 dB of SNR and an important performance gap for the remainder SNR values. For the strategies with $Q = 0$ and $\Delta_f = 4$, and $Q = 3$ and $\Delta_f = 7$, these performance gains increase with the SNR, whereas HI reduces the gap for very high SNRs and the configuration $Q = 2$ and $\Delta_f = 5$.

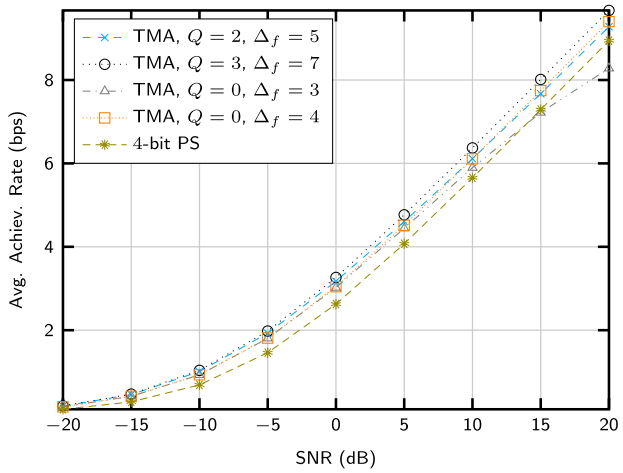

FIGURE 10. Achievable rate (bps) vs. SNR (dB) for $\Delta_f = \{3, 4\}$ and the symbol configuration in Sec. V-A with penalty parameter $\gamma = 1$, and for $Q = \{2, 3\}$, $\Delta_f = \{5, 7\}$ and the symbol configuration in Sec. V-B. The number of RF chains and antennas are $N_{\mathrm{RF}} = 4$ and $M = 64$.

We now evaluate the effects derived from changing the number of transmit antennas and RF chains. In particular, we use the simulation parameters of Table 2, but reducing the number of RF chains ($N_{\mathrm{RF}} = 4$) to obtain the results in Fig. 10. Furthermore, the penalty parameter in (38) is set to $\gamma = 1$ in this scenario. We observe that the impact of reducing the available degrees of freedom for hybrid precoding is larger for TMA strategies since the performance gap with respect to the curve representing the PS-based analog network reduces compared to Fig. 6 and Fig. 7. In the TMA network this reduction does not only lead to smaller equivalent channel gains but also reduces the flexibility of the baseband precoder to combat the SR. Besides the smaller number of RF chains, we additionally reduce the number of

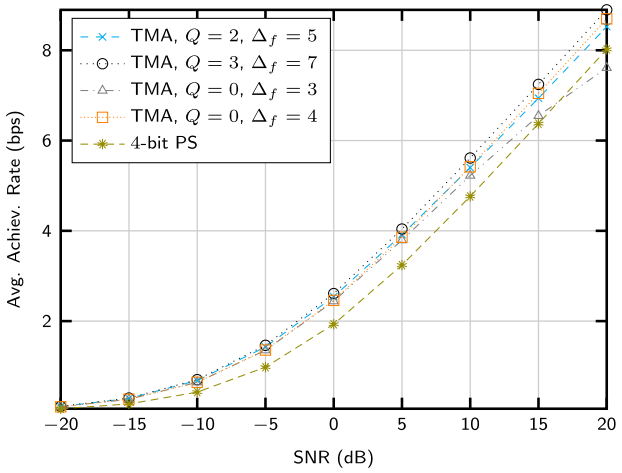

FIGURE 11. Achievable rate (bps) vs. SNR (dB) for $\Delta_f = \{3, 4\}$ and the symbol configuration in Sec. V-A with penalty parameter $\gamma = 1$, and for $Q = \{2, 3\}$, $\Delta_f = \{5, 7\}$ and the symbol configuration in Sec. V-B. The number of RF chains and antennas are $N_{\mathrm{RF}} = 4$ and $M = 32$.

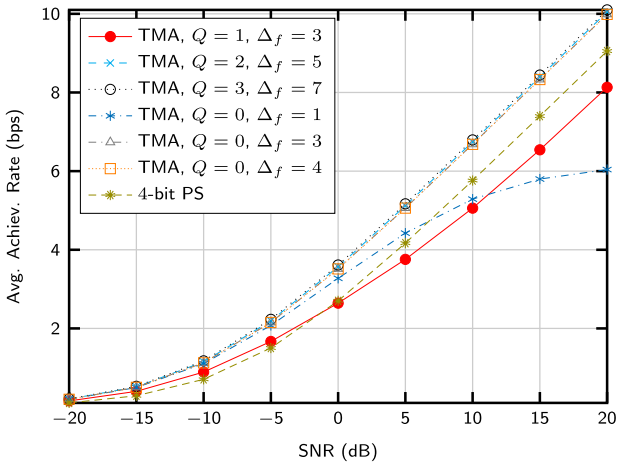

FIGURE 12. Achievable rate (bps) vs. SNR (dB) for $\Delta_f = \{1, 3, 4\}$ and the symbol configuration in Sec. V-A with penalty parameter $\gamma = 1$, and for $Q = \{1, 2, 3\}$, $\Delta_f = \{3, 5, 7\}$ and the symbol configuration in Sec. V-B. The number of significant harmonics is $K = 5$.

antennas to $M = 32$ in Fig. 11. In this case, the number of RF chains provides more flexibility for the hybrid precoding compared to the scenario with $M = 64$. Therefore, using the proposed TMA network and hybrid precoding strategies we observe performance gains similar to those achieved in Fig. 6 and Fig. 7.

In Fig. 12 we show the effect of reducing the number of significant harmonics, that is $K = 5$, while the rest of parameters are those in Table 2. This condition applies to practical scenarios for TMA networks with more elaborated circuitry, aiming at reducing the SR. Observe that the performance for both symbol configurations increases for the whole SNR regime when $\Delta_f \geq 3$. That is, the harmonic interference is completely removed. Contrarily, for the symbol configuration of Sec. VI-A and $\Delta_f = 1$, the average achievable rate saturates for high SNR values. We can also conclude

that, as $\Delta_f \geq \frac{K+1}{2}$, the two symbol configurations provide similar average per-subcarrier performance. Furthermore, all the curves present increased performance with respect to the experiments in Fig. 6 and Fig. 7. Consequently, reduced SR improves the performance gains compared to the PS-based approach.

C. BEAM PATTERN

Side lobes are usually considered in the antenna array literature [39], [40], and provide a different perspective to evaluate our hybrid precoding designs. To illustrate this issue, we provide an example of beam pattern in Fig. 13 for the central carrier of a channel realization with a single channel path $N_p = 1$ and $\vartheta = \frac{\pi}{3}$. We compare the beam patterns for hybrid precoding with the optimum, in terms of achievable rate, digital precoder. As can be appreciated, the flexibility to model the radiation pattern provided by the baseband precoders is not enough to compensate the undesired side lobes introduced by the analog precoding matrices. Indeed, the main lobe for hybrid precoders is not perfectly aligned with the digital one. Remarkably, the hybrid precoder of Sec. VI-A presents a smaller number of weaker side lobes, whereas for the hybrid precoder of Sec. VI-B side lobes are similar to those obtained with the PS-based scheme.

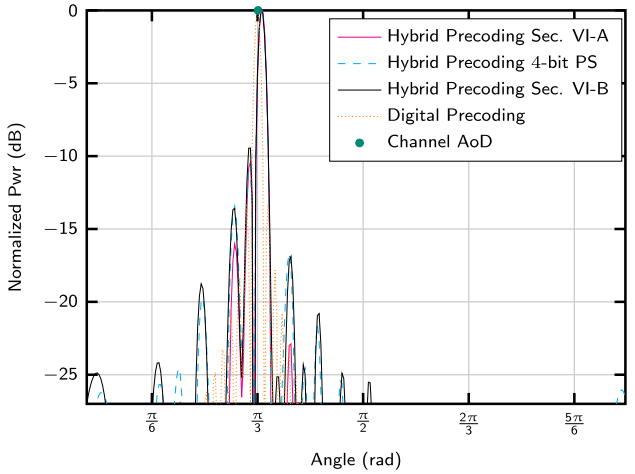

FIGURE 13. Beam pattern example of the different precoding strategies. The number of channel paths is $N_p = 1$ and $\vartheta = \frac{\pi}{3}$. The remaining setup parameters are provided in Table 2.

It is clear that we must design hybrid precoders such that the beam pattern is similar or equal to that of the digital precoder. When this is not the case, the hybrid approaches require more transmit power to obtain the achievable rates reached with the digital design.

VIII. CONCLUSION

TMA hybrid precoding with SPDT switches in the analog domain has been considered for the transmission of OFDM wideband signals. The posed TMA analog network generates harmonic replicas which overlap when handling wideband signals. In this work, we pose a flexible design of the OFDM transmitted symbols to combat such harmonic interference. Following this design, we allow different OFDM symbol configurations to be adapted according to the channel conditions, transmit power available, or underlying TMA features. The use of these OFDM symbols and a SPDT TMA analog network is next taken into account to design suitable hybrid precoders. Contrary to designs with conventional phased array precoders, we consider the power inefficiencies introduced by the hardware. The numerical results show the good performance achieved with the TMA scheme proposed, while exhibiting an outstanding power efficiency.

APPENDIX I. PARAMETER CONFIGURATION

A. REMOVING HI FOR THE FUNDAMENTAL MODE

Here we show that the configuration $\Delta_f = \frac{K+1}{2}$, with Δ_t such that $\gcd(\Delta_f, \Delta_t) = 1$ removes the overlapping of harmonic replicas for the frequencies containing data.

First, let us generate a set of tuples satisfying $a(q, \ell) = i$ from a starting tuple (q_0, ℓ_0) using Bézout's identity, that is,

$$\mathcal{B}_i = \left\{ q_0 - k\frac{\Delta_f}{\gcd(\Delta_f, \Delta_t)}, \ell_0 + k\frac{\Delta_t}{\gcd(\Delta_f, \Delta_t)} \right\} \quad (53)$$

for $k \in \mathbb{Z}$. Observe, however, that $\mathcal{H}_i \subset \mathcal{B}_i$ due to the constraints imposed over ℓ and q on (14). Thus, in our formulation k must satisfy the following conditions

$$-\ell_0\frac{\gcd(\Delta_f, \Delta_t)}{\Delta_f} \leq k \leq (L-1-\ell_0)\frac{\gcd(\Delta_f, \Delta_t)}{\Delta_f}$$
$$|k| \leq \left(\frac{N}{2} - |q_0|\right)\frac{\gcd(\Delta_f, \Delta_t)}{\Delta_f}.$$

Consider the subcarrier index i containing the symbol ℓ_0 for the harmonic $q_0 = 0$, with $\Delta_f = \frac{K+1}{2}$. Hence, any harmonic index q_1 contained in the i-th subcarrier satisfies

$$q_1 = \frac{i}{\Delta_t} - \ell_1\frac{K+1}{2\Delta_t} = (\ell_0 - \ell_1)\frac{K+1}{2\Delta_t}. \quad (54)$$

Now, under the assumption $\gcd(\Delta_f, \Delta_t) = 1$, feasible options for $\ell_0 - \ell_1$ satisfy $|\ell_0 - \ell_1| \geq \Delta_t$ to provide integer values for q_1. Then, considering negligible harmonics for $|q| > \frac{K-1}{2}$, the only significant index q_1 is obtained when $\ell_0 = \ell_1$. Therefore, the data symbol ℓ_0 corresponding to the fundamental mode at frequency i does not suffer interference. Moreover, $\Delta_f = \frac{K+1}{2}$ is the smaller frequency separation ensuring this feature.

B. COMPLETELY REMOVING HI

It is also interesting to extend the previous condition for all the frequencies, i.e., removing the interference also for the harmonic replicas filling the free subcarriers. To that end, we set $\Delta_f = K$ and Δ_t such that $\gcd(\Delta_f, \Delta_t) = 1$. Thus, recalling our assumption of negligible harmonics for $|q| > \frac{K-1}{2}$, this reasoning leads to irrelevant interference levels. To show uniqueness of the harmonics for the frequency i, consider a tuple (q_0, ℓ_0) with $|q_0| \leq \frac{K-1}{2}$, and a different pair $(q_1, \ell_1) \neq (q_0, \ell_0)$ satisfying $a(q_1, \ell_1) = i$. We now write

the equality

$$q_0\Delta_t + \ell_0\Delta_f = q_1\Delta_t + \ell_1\Delta_f,$$

or equivalently

$$q_1 = (\ell_0 - \ell_1)\frac{\Delta_f}{\Delta_t} + q_0.$$

Taking into account that Δ_t and Δ_f are co-prime integers, $|\ell_0 - \ell_1| \geq \Delta_t$ and, due to the fact that $|q_0| \leq \frac{K-1}{2}$, the values for the harmonic index q_1 satisfy

$$|q_1| \geq \frac{K+1}{2} > \frac{K-1}{2}. \tag{55}$$

That is, q_1 indices corresponding to negligible harmonics. The former equation also reveals that $\Delta_f = K$ is the minimum frequency separation to avoid overlapping among any harmonic replicas.

REFERENCES

[1] T. S. Rappaport, S. Sun, R. Mayzus, H. Zhao, Y. Azar, K. Wang, G. N. Wong, J. K. Schulz, M. Samimi, and F. Gutierrez, "Millimeter wave mobile communications for 5G cellular: It will work!" *IEEE Access*, vol. 1, pp. 335–349, 2013.

[2] R. W. Heath, N. Gonzalez-Prelcic, S. Rangan, W. Roh, and A. M. Sayeed, "An overview of signal processing techniques for millimeter wave MIMO systems," *IEEE J. Sel. Topics Signal Process.*, vol. 10, no. 3, pp. 436–453, Apr. 2016.

[3] R. Mendez-Rial, C. Rusu, N. Gonzalez-Prelcic, A. Alkhateeb, and R. W. Heath, "Hybrid MIMO architectures for millimeter wave communications: Phase shifters or switches?" *IEEE Access*, vol. 4, pp. 247–267, 2016.

[4] A. Alkhateeb and R. W. Heath, "Frequency selective hybrid precoding for limited feedback millimeter wave systems," *IEEE Trans. Commun.*, vol. 64, no. 5, pp. 1801–1818, May 2016.

[5] J. P. Gonzalez-Coma, W. Utschick, and L. Castedo, "Hybrid LISA for wideband multiuser millimeter-wave communication systems under beam squint," *IEEE Trans. Wireless Commun.*, vol. 18, no. 2, pp. 1277–1288, Feb. 2019.

[6] K. Venugopal, N. Gonzalez-Prelcic, and R. W. Heath, "Optimal frequency-flat precoding for frequency-selective millimeter wave channels," *IEEE Trans. Wireless Commun.*, vol. 18, no. 11, pp. 5098–5112, Nov. 2019.

[7] Y. Chen, D. Chen, T. Jiang, and L. Hanzo, "Channel-covariance and angle-of-departure aided hybrid precoding for wideband multiuser millimeter wave MIMO systems," *IEEE Trans. Commun.*, vol. 67, no. 12, pp. 8315–8328, Dec. 2019.

[8] R. Zhang, W. Zou, Y. Wang, and M. Cui, "Hybrid precoder and combiner design for single-user mmWave MIMO systems," *IEEE Access*, vol. 7, pp. 63818–63828, 2019.

[9] H. Yuan, J. An, N. Yang, K. Yang, and T. Q. Duong, "Low complexity hybrid precoding for multiuser millimeter wave systems over frequency selective channels," *IEEE Trans. Veh. Technol.*, vol. 68, no. 1, pp. 983–987, Jan. 2019.

[10] T. Mir, M. Zain Siddiqi, U. Mir, R. Mackenzie, and M. Hao, "Machine learning inspired hybrid precoding for wideband millimeter-wave massive MIMO systems," *IEEE Access*, vol. 7, pp. 62852–62864, 2019.

[11] K. Satyanarayana, M. El-Hajjar, A. A. M. Mourad, and L. Hanzo, "Multi-user full duplex transceiver design for mmWave systems using learning-aided channel prediction," *IEEE Access*, vol. 7, pp. 66068–66083, 2019.

[12] H. Li, M. Li, and Q. Liu, "Hybrid beamforming with dynamic subarrays and low-resolution PSs for mmWave MU-MISO systems," *IEEE Trans. Commun.*, vol. 68, no. 1, pp. 602–614, Jan. 2020.

[13] M. C. Scardelletti and G. E. Ponchak, "RF MEMS phase shifters and their application in phase array antennas," in *Proc. IEEE Annu. Conf. Wireless Micrwave Technol.*, Apr. 2005, p. 37.

[14] W. B. Abbas, F. Gomez-Cuba, and M. Zorzi, "Millimeter wave receiver efficiency: A comprehensive comparison of beamforming schemes with low resolution ADCs," *IEEE Trans. Wireless Commun.*, vol. 16, no. 12, pp. 8131–8146, Dec. 2017.

[15] J. P. Gonzalez-Coma, R. Maneiro-Catoira, and L. Castedo, "Hybrid precoding with time-modulated arrays for mmwave MIMO systems," *IEEE Access*, vol. 6, pp. 59422–59437, 2018.

[16] J. C. Bregains, J. Fondevila-Gomez, G. Franceschetti, and F. Ares, "Signal radiation and power losses of time-modulated arrays," *IEEE Trans. Antennas Propag.*, vol. 56, no. 6, pp. 1799–1804, Jun. 2008.

[17] M. H. Mazaheri, M. Fakharzadeh, and M. Akbari, "Efficiency enhancement of time-modulated arrays with optimized switching sequences," *IEEE Trans. Antennas Propag.*, vol. 66, no. 7, pp. 3411–3420, Jul. 2018.

[18] G. Bogdan, Y. Yashchyshyn, and M. Jarzynka, "Time-modulated antenna array with lossless switching network," *IEEE Antennas Wireless Propag. Lett.*, vol. 15, pp. 1827–1830, 2016.

[19] G. Bogdan, K. Godziszewski, Y. Yashchyshyn, C. H. Kim, and S.-B. Hyun, "Time modulated antenna array for real-time adaptation in wideband wireless systems—Part I: Design and characterization," *IEEE Trans. Antennas Propag.*, early access, Mar. 2019, doi: 10.1109/TAP.2019.2902755.

[20] R. Maneiro-Catoira, J. Bregains, J. A. Garcia-Naya, and L. Castedo, "Time-modulated phased array controlled with nonideal bipolar squared periodic sequences," *IEEE Antennas Wireless Propag. Lett.*, vol. 18, no. 2, pp. 407–411, Feb. 2019.

[21] R. Maneiro-Catoira, J. Brégains, J. A. García-Naya, and L. Castedo, "Time-modulated array beamforming with periodic stair-step pulses," *Signal Process.*, vol. 166, Jan. 2020, Art. no. 107247. [Online]. Available: http://www.sciencedirect.com/science/article/pii/S0165168419302932

[22] Q. Chen, J.-D. Zhang, W. Wu, and D.-G. Fang, "Enhanced single-sideband time-modulated phased array with lower sideband level and loss," *IEEE Trans. Antennas Propag.*, vol. 68, no. 1, pp. 275–286, Jan. 2020.

[23] J. P. Gonzalez-Coma and L. Castedo, "Power efficient scheduling and hybrid precoding for time modulated arrays," *IEEE Access*, vol. 8, pp. 21063–21076, 2020.

[24] Y. Li, S. Ghafoor, K. Satyanarayana, M. El-Hajjar, and L. Hanzo, "Analogue wireless beamforming exploiting the fiber-nonlinearity of radio over fiber-based C-RANs," *IEEE Trans. Veh. Technol.*, vol. 68, no. 3, pp. 2802–2813, Mar. 2019.

[25] References: RFSW6024, RF1630, RFSW1012. *Qorvo*. Accessed: Mar. 2020. [Online]. Available: http://www.qorvo.com

[26] P. Smulders, "Statistical characterization of 60-GHz indoor radio channels," *IEEE Trans. Antennas Propag.*, vol. 57, no. 10, pp. 2820–2829, Oct. 2009.

[27] G. Femenias and F. Riera-Palou, "Scheduling and resource allocation in downlink multiuser MIMO-OFDMA systems," *IEEE Trans. Commun.*, vol. 64, no. 5, pp. 2019–2034, May 2016.

[28] A. A. Rodríguez, F. P. González, J. C. Sueiro, R. L. Valcarce, C. M. Nartallo, and F. P. Cruz, *Comunicaciones Digitales*. Upper Saddle River, NJ, USA: Prentice-Hall, 2007. [Online]. Available: https://books.google.es/books?id=0Rn3PQAACAAJ

[29] A. A. M. Saleh and R. Valenzuela, "A statistical model for indoor multipath propagation," *IEEE J. Sel. Areas Commun.*, vol. 5, no. 2, pp. 128–137, Feb. 1987.

[30] H. L. Van Trees, *Optimum Array Processing*. Hoboken, NJ, USA: Wiley, Mar. 2002, doi: 10.1002/0471221104.

[31] A. S. Y. Poon and M. Taghivand, "Supporting and enabling circuits for antenna arrays in wireless communications," *Proc. IEEE*, vol. 100, no. 7, pp. 2207–2218, Jul. 2012.

[32] Z. Cao, Q. Ma, A. B. Smolders, Y. Jiao, M. J. Wale, C. W. Oh, H. Wu, and A. M. J. Koonen, "Advanced integration techniques on broadband millimeter-wave beam steering for 5G wireless networks and beyond," *IEEE J. Quantum Electron.*, vol. 52, no. 1, pp. 1–20, Jan. 2016.

[33] D. Liu, U. Pfeiffer, J. Grzyb, and B. Gaucher, *Advanced Millimeter-wave Technologies: Antennas, Packaging and Circuits*. Hoboken, NJ, USA: Wiley, 2009. [Online]. Available: https://books.google.es/books?id=t5d4-_h1TBQC

[34] S. Zihir, O. D. Gurbuz, A. Kar-Roy, S. Raman, and G. M. Rebeiz, "60-GHz 64- and 256-elements wafer-scale phased-array transmitters using full-reticle and subreticle stitching techniques," *IEEE Trans. Microw. Theory Techn.*, vol. 64, no. 12, pp. 4701–4719, Dec. 2016.

[35] X. Xie, R. Xu, B. Yan, Y. Zhang, and W. Lin, "A novel millimeter-wave power combining circuit," *Int. J. Infr. Millim. Waves*, vol. 26, no. 10, pp. 1453–1464, Sep. 2005, doi: 10.1007/s10762-005-8443-2.

[36] K. Yin, K. Zhang, and J. Xu, "Characterization and design of millimeter-wave full-band waveguide-based spatial power divider/combiner," *Prog. Electromagn. Res. C*, vol. 50, pp. 65–74, 2014, doi: 10.2528/PIERC14031604.

[37] Q. Shi, M. Razaviyayn, Z.-Q. Luo, and C. He, "An iteratively weighted MMSE approach to distributed sum-utility maximization for a MIMO interfering broadcast channel," *IEEE Trans. Signal Process.*, vol. 59, no. 9, pp. 4331–4340, Sep. 2011.
[38] R. Maneiro-Catoira, J. Brégains, J. García-Naya, and L. Castedo, "Time modulated arrays: From their origin to their utilization in wireless communication systems," *Sensors*, vol. 17, no. 3, p. 590, Mar. 2017.
[39] I. A. Hemadeh, K. Satyanarayana, M. El-Hajjar, and L. Hanzo, "Millimeter-wave communications: Physical channel models, design considerations, antenna constructions, and link-budget," *IEEE Commun. Surveys Tuts.*, vol. 20, no. 2, pp. 870–913, 2nd Quart., 2018.
[40] S. Orfanidis. (2016). *Electromagnetic Waves and Antennas*. [Online]. Available: http://eceweb1.rutgers.edu/~orfanidi/ewa/

JOSÉ P. GONZÁLEZ-COMA (Member, IEEE) was born in Marín, Spain. He received the degree in computer engineering and the Ph.D. degree from the University of A Coruña, Spain, in 2009 and 2015, respectively. He was appointed as a Visiting Researcher at the Associate Institute for Signal Processing, Technische Universität München, Germany, in 2012, and the Signal Processing in Communications Group (UVIGO), Spain, in 2017. Since 2017, he has been with the Research Center on Information and Communication Technologies, University of A Coruña, where he is currently a Postdoctoral Researcher. He received the FPI Grant from the Ministerio de Ciencia e Innovación. His main research interests are in channel estimation and precoding in massive multi-in multi-out systems, and millimeter-wave communications.

LUIS CASTEDO (Senior Member, IEEE) received the Ph.D. degree in telecommunication engineering from the Technical University of Madrid, Spain. Since 1994, he has been a Faculty Member of the Department of Computer Engineering, University of A Coruña (UDC), Spain, where he became a Professor, in 2001, and acted as the Chairman, from 2003 to 2009. He had previously held several research appointments at the University of Southern California (USC) and École supérieure d'électricité (SUPELEC). From 2014 to 2018, he has been the Manager of the Communications and Electronic Technologies (TEC) Program of the State Research Agency of Spain. He is currently a Professor with the UDC. He is the coauthor of more than 300 papers in peer-reviewed international journals and conferences. He has also been the principal investigator of more than 50 research projects funded by public organizations and private companies. He has advised 16 Ph.D. degree dissertations. His research interests are signal processing, coding, hardware prototyping, and experimental evaluation in wireless communications engineering. His papers have received three best student paper awards from the IEEE/ITG Workshop on Smart Antennas, in 2007, the IEEE International Workshop on Signal Processing Advances in Wireless Communications, in 2013, and the IEEE International Conference on the Internet of Things (iThings), in 2017. He was the General Co-Chair of the Eighth IEEE Sensor Array and Multichannel Signal Processing Workshop, in 2014, and the 27th European Signal Processing Conference, in 2019.